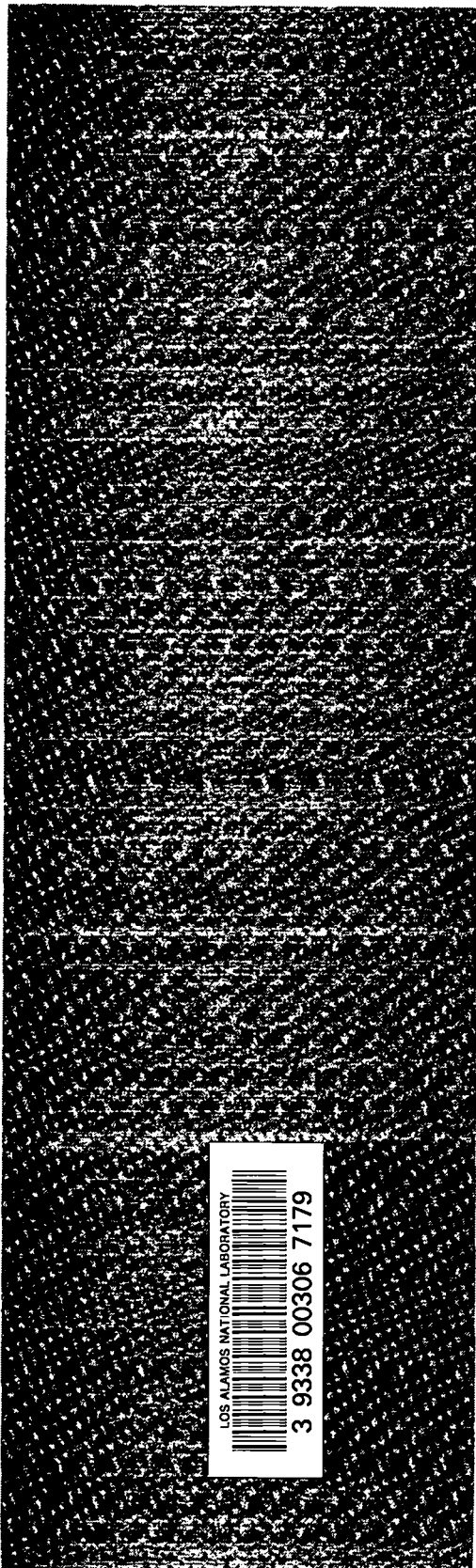


**REPRODUCTION  
COPY**

**C.3**



*DSD Technology:*

*A Detonation Reactive Huygens Code*

**Los Alamos**

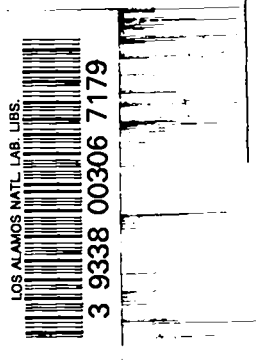
*Los Alamos National Laboratory is operated by the University of California for the United States Department of Energy under contract W-7405-ENG-36.*

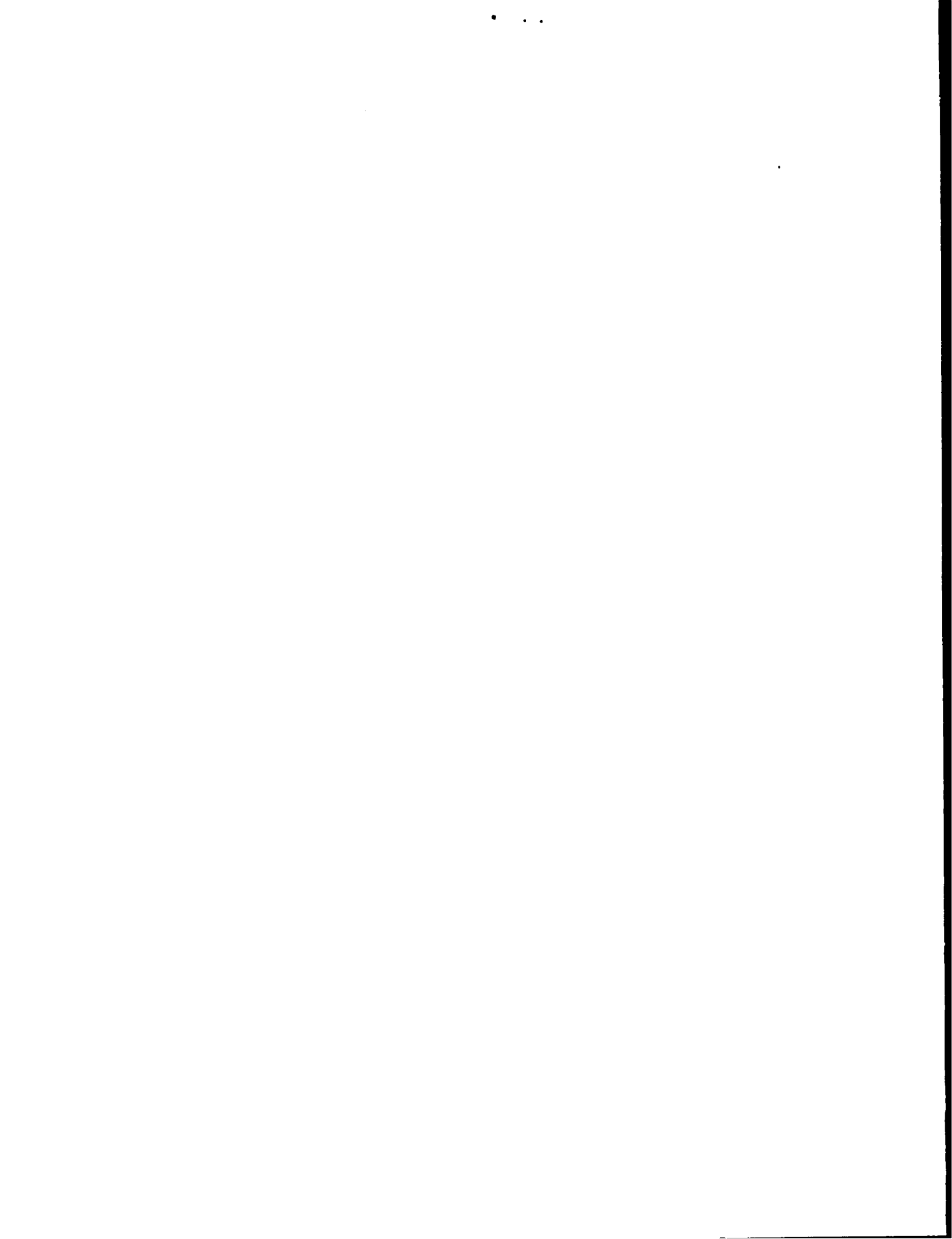
*An Affirmative Action/Equal Opportunity Employer*

*This report was prepared as an account of work sponsored by an agency of the United States Government. Neither The Regents of the University of California, the United States Government nor any agency thereof, nor any of their employees, makes any warranty, express or implied, or assumes any legal liability or responsibility for the accuracy, completeness, or usefulness of any information, apparatus, product, or process disclosed, or represents that its use would not infringe privately owned rights. Reference herein to any specific commercial product, process, or service by trade name, trademark, manufacturer, or otherwise, does not necessarily constitute or imply its endorsement, recommendation, or favoring by The Regents of the University of California, the United States Government, or any agency thereof. The views and opinions of authors expressed herein do not necessarily state or reflect those of The Regents of the University of California, the United States Government, or any agency thereof.*

*DSD Technology:  
A Detonation Reactive Huygens Code*

*John Bdzil  
Wildon Fickett*





## CONTENTS

I. INTRODUCTION . . . . .	1
II. GEOMETRY AND NOTATION . . . . .	3
III. EQUATIONS . . . . .	6
IV. INPUT AND OUTPUT . . . . .	9
V. SAMPLE PROBLEMS . . . . .	18
VI. EXACT SOLUTIONS . . . . .	33
VII. CODE STRUCTURE . . . . .	38
REFERENCES . . . . .	42
Appendix A. SCALING . . . . .	43
Appendix B. DETONATION FAILURE MODELS . . . . .	44

# DSD TECHNOLOGY: A DETONATION REACTIVE HUYGENS CODE

by

John Bdzil and Wildon Fickett

## ABSTRACT

The length of the reaction zone strongly influences the speed of propagation of detonation in multi-dimensional explosive pieces. Detonation Shock Dynamics (DSD) properly accounts for these effects in detonation wave-spreading problems when the radius of curvature of the multi-dimensional detonation shock is large compared to the explosive's reaction-zone length. This report is a user manual for our two-dimensional implementation of this method; a FORTRAN subroutine called DSD Technology.

---

## I. INTRODUCTION

Modeling detonation propagation in complex shaped explosive pieces is an important problem in the design process for explosively powered devices. The computational problems that arise are difficult, because the physics important to the problem occurs on many disparate length scales. For example, the device size is typically many orders of magnitude larger than the size of the explosive's detonation reaction zone. One of the principal shortcomings of the computer models that are presently used for multi-dimensional explosive engineering design is their inadequate treatment of the explosive's detonation reaction zone. Current uniform-grid methods lack the resolution to calculate both the broad gas expansion region and simultaneously the thin reaction zone with reasonable detail. Consequently, detailed calculations that resolve the reaction zone are seldom performed. Typically, the reaction zone is assumed to be infinitesimally thin and its dynamics is modeled by a scale independent detonation Huygens construction. This model assumes that detonation propagation is purely a geometric problem; the multi-dimensional detonation wave is a shock that expands normal to itself at the constant Chapman-Jouguet detonation speed,  $D_{CJ}$ . When the detonation reaction zone is exceedingly short compared to a representative dimension of the explosive piece, this simple model yields good results.

In recent years, concerns about accidental initiation of detonation have led to the use of insensitive explosives; explosives with reaction zones orders of magnitude longer. Because

of the increased length of their reaction zones, the detonation speed departs significantly from  $D_{CJ}$ . For example, for these explosives the detonation speed is slower for expanding waves than for plane ones, and near edges the detonation speed can be significantly reduced; this reduction causes the detonation wave to become curved. Drawing on recent theoretical research on multi-dimensional detonation, we have developed a theory called DSD that incorporates the explosive's scale dependency; this theory allows us to model finite reaction zone effects. DSD is the acronym for the "Detonation Shock Dynamics" theory<sup>1,2</sup> developed by John Bdzil and Scott Stewart. This theory provides a recipe for propagating a detonation wave front without calculating the flow behind it. A central result of the theory is that the normal velocity  $D$  of the wave front at any point depends only on the wave curvature  $\kappa$  at that point. This has the effect of reducing the dimensionality of the detonation propagation problem by one. Thus a problem with either a plane or axis of symmetry (a two-dimensional problem) becomes a one-dimensional problem. A function  $D(\kappa)$  characterizes each explosive and is considered to be a material property. This function can be calculated theoretically if the equation of state and reaction rates are known but is obtained in practice from simple calibration experiments.

DSD is a low-frequency (long transverse wavelength) asymptotic theory. The governing equation is a parabolic partial-differential equation (PDE), similar in form to Burgers' equation (see Ref. 3, ch. 4), but with a complicated coefficient involving integrals over the solution. For the theory to apply, the radius of curvature of the front must be much larger than the length of the reaction zone.

The theory is analogous to Whitham's "Geometrical Shock Dynamics" theory, (Ref. 3, ch. 8), but applies to detonation waves instead of inert shocks. The mathematical form of "Geometrical Shock Dynamics" (a hyperbolic theory) is different from DSD (a parabolic theory). This difference in form follows from the fact that inert shocks decelerate as they expand whereas detonations accelerate.

As  $D(\kappa)$  drops below  $D_{CJ}$ , the thermodynamic state point from which the explosive products undergo expansion changes. The Chapman-Jouguet state is not the proper starting state. Given  $D(\kappa)$  and a compatible equation of state for the products, the proper starting state for the numerical computation of the products region (the working fluid) can be calculated. Since  $D$  typically varies along the shock, the starting state for the explosive products is different at the center and edge of the explosive piece. Thus by incorporating the reaction zone effects into the detonation propagation model, DSD also yields the proper starting point for the expansion of each parcel of explosive product.

Brian Lambourn and Damian Swift<sup>4</sup> at the Atomic Weapons Establishment (AWE) in England have developed a theory similar to DSD. They call their implementation of the theory the Whitham-Bdzil-Lambourn (WBL) detonation model.

The plan of this report is as follows. The problem geometry and intrinsic coordinate representation that we use are presented in Chap. II. The evolution equation for the shock, the boundary conditions and  $D(\kappa)$  functions are discussed in Chap. III. In Chap. IV we describe the structure of the input deck that is used to set up problems. Selected output from seven sample problems is presented and discussed in Chap. V. Chapter VI is a brief tutorial on the DSD method. The structure of the code is described in Chap. VII. The scaled variables used in the code are described in Appendix A. The detonation failure models currently implemented in the code are described in Appendix B.

## II. GEOMETRY AND NOTATION

The detonation is assumed to have the usual Zeldovich-von Neumann-Doering (ZND) structure, that is, a shock followed by a reaction zone. The theory tracks the leading shock, which we will refer to as the shock.

The governing equations are written in the intrinsic coordinates shown in Fig. 2.1. This is a key step in constructing a tractable and transparent theory. The independent variables are  $\xi$ , the distance (arclength) along the shock, and the time  $t$ . The dependent variable is  $\phi$ , the inclination of the shock, defined as the angle between the vertical and the outward (*i.e.*, drawn in the direction of propagation) normal to the shock, with  $\phi$  positive for clockwise rotation of the normal from the vertical.

The laboratory coordinates  $x$  and  $y$  of the shock (cartesian coordinates in the frame with the undisturbed explosive at rest) at a given time  $t$  are related to the intrinsic coordinates  $\xi$  and  $\phi$  by

$$x(\xi, t) = x_e(t) + \int_0^\xi \cos \phi(\xi', t) d\xi' \quad , \quad (2.1a)$$

$$y(\xi, t) = y_e(t) - \int_0^\xi \sin \phi(\xi', t) d\xi' \quad . \quad (2.1b)$$

The integration begins at an edge point  $x_e(t)$ ,  $y_e(t)$  where  $\xi$  is assigned the value zero.

We use the term body to denote the piece of explosive in which the wave propagates. For our purposes we regard the body as bounded by a specified initial shock and two edges, as shown in Fig. 2.2. The edges are the two physical edges of the explosive between which the shock propagates.

We treat only the (mathematically) "one-dimensional" case, that is, with one space and one time variable. There are two possible symmetries which we refer to by the names slab and cylinder. These are defined as follows:

### (1) Slab

Fig. 2.2 is a cross section of a body of infinite extent in the direction normal to the paper; all curves (edges and shock) are cylindrical surfaces with generators normal to the paper.

### (2) Cylinder

Fig. 2.2 is a cross section of a figure of revolution about the centerline  $x = 0$ .

For either of these geometries, the terms we use to describe the shape of the shock or an edge will refer to the section in the plane of the paper. Thus, for example, a shock



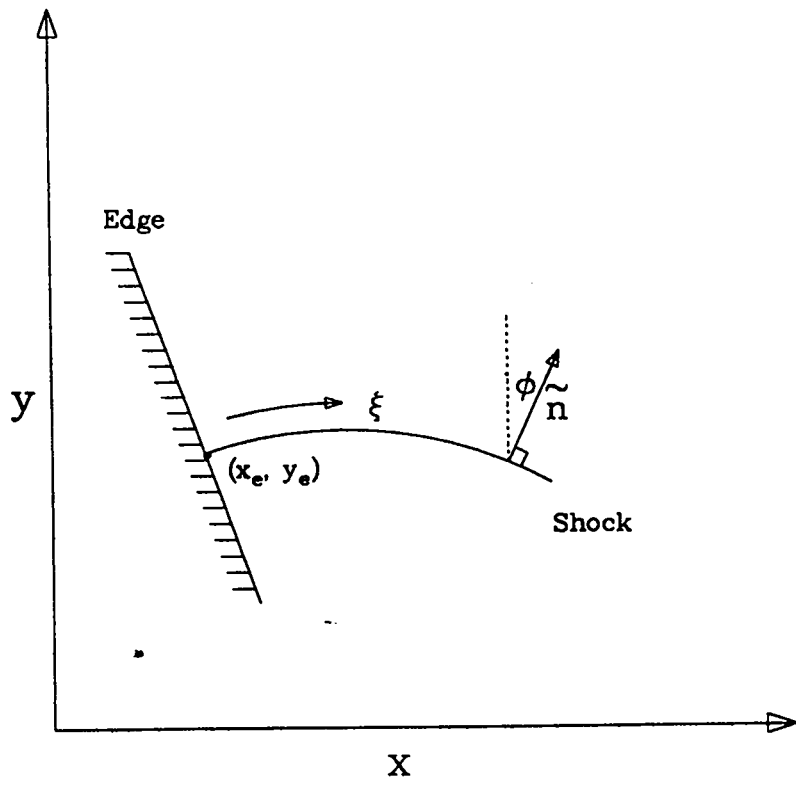


Fig. 2.1 Intrinsic coordinates.

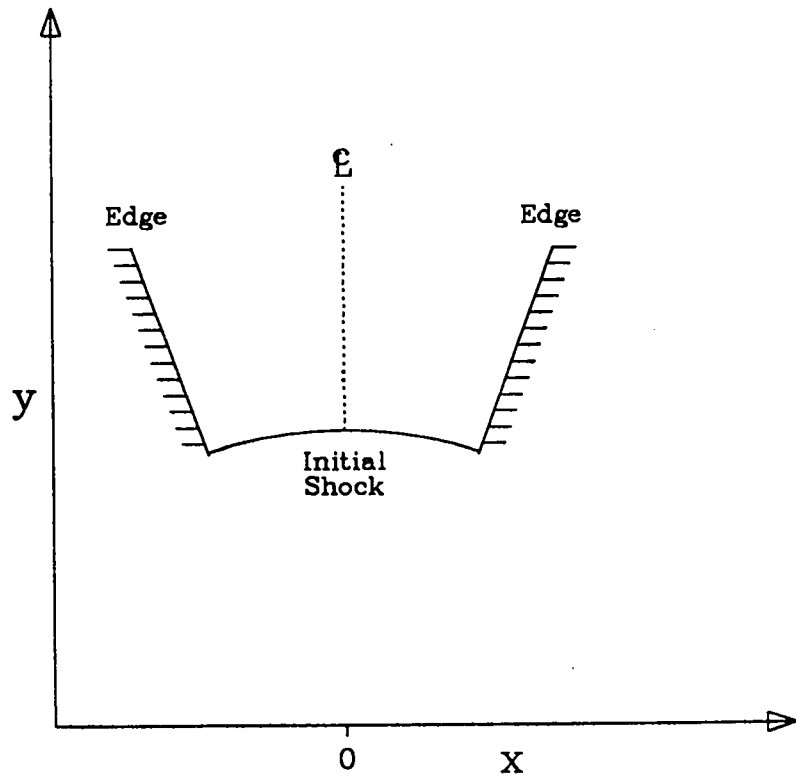


Fig. 2.2 The body.

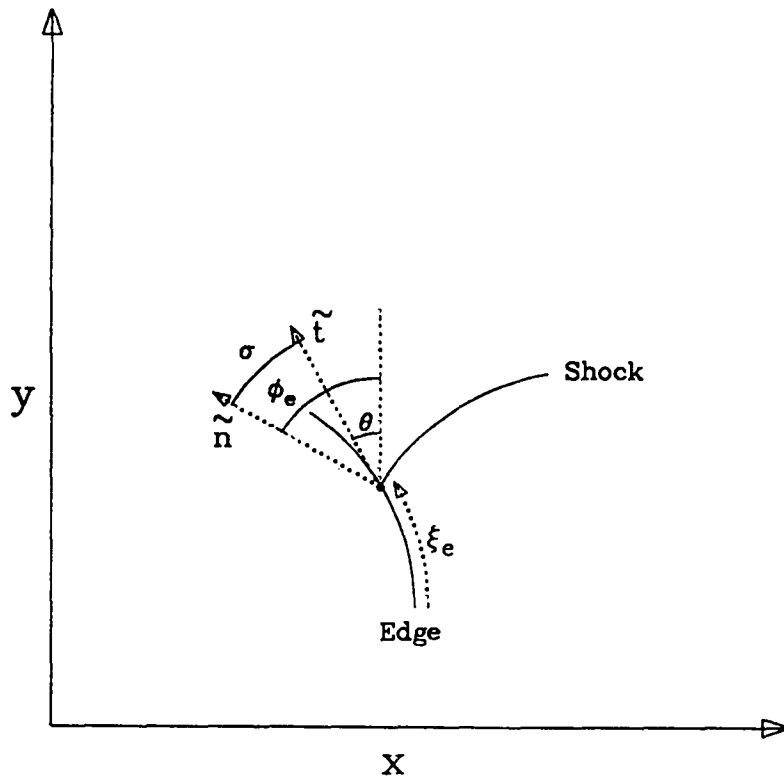


Fig. 2.3 The edge and associated angles. The directions  $\tilde{t}$  and  $\tilde{n}$  are the tangent to the edge and the normal to the shock.

described as an arc of a circle would be in reality a cylindrical shock in the slab case and a spherical shock in the cylinder case.

The left edge is the reference edge; along it the shock arclength  $\xi$  is assigned the value zero. We use subscript  $e$  to denote an edge; in the absence of qualification, this refers to the reference edge. Figure 2.3 shows an edge and some associated angles. We denote by  $\theta$  the inclination of the edge, defined as the angle between the vertical and the tangent to the edge, with  $\theta$  positive for clockwise rotation of the tangent from the normal. At the edge we have the shock inclination  $\phi_e$  and the normal shock velocity  $D_e$ . It is useful to define another angle  $\sigma$ , which measures the deviation from normal incidence. It is the angle between the wave normal at the edge and the tangent to the edge, that is

$$\sigma = \phi_e - \theta \quad , \quad (2.2)$$

so that  $\sigma = 0$  for normal incidence. The phase velocity  $D_{ph}$  of the intersection point with the edge is given by

$$D_{ph} = \frac{d\xi_e}{dt} = \frac{D_e}{\cos \sigma} \quad , \quad (2.3)$$

where  $\xi_e$  is arclength along the edge, increasing in the direction of propagation. The

solution of Eq. (2.3),  $\xi_e(t)$  and the prescribed edge shape,  $\theta(\xi_e)$  combine to yield the edge coordinates  $x_e(t)$ ,  $y_e(t)$

$$x_e(t) = x_e(0) + \int_0^{\xi_e} \sin \theta(\xi'_e) d\xi'_e \quad , \quad (2.4a)$$

$$y_e(t) = y_e(0) + \int_0^{\xi_e} \cos \theta(\xi'_e) d\xi'_e \quad . \quad (2.4b)$$

### III. EQUATIONS

#### (1) Equations of Motion

The governing equations for  $\phi(\xi, t)$  are

$$\phi_t + B\phi_\xi = -D_\xi = -D'(\kappa)(\phi_{\xi\xi} + kS_\xi) \quad (3.1a)$$

$$B \equiv \int_0^\xi D\phi_\xi d\xi + D_e \tan \sigma \quad (3.1b)$$

$$\kappa \equiv \phi_\xi + S \quad (3.1c)$$

$$S \equiv \sin \phi/x \quad (3.1d)$$

$$k = 0/1 \text{ for slab/cylinder symmetry} \quad . \quad (3.1e)$$

The shock kinematics is described by Eq. (3.1a), which resembles Burgers' equation

$$u_t + uu_x = \nu u_{xx} \quad , \quad (3.2)$$

with the coefficient  $B$  the propagation speed and  $-D'(\kappa) \equiv -dD(\kappa)/d\kappa$  the "viscosity"  $\nu$ . The first (integral) term in  $B$  represents the change in shock surface from wave spreading, and the second term the change from the intersection at the edge (note that the second term is zero for normal incidence). For slab symmetry, the curvature  $\kappa$  is just the reciprocal of the local radius of curvature of the shock.

The function  $D(\kappa)$  characterizes the explosive dynamics and must be specified by the user. Typically, it is determined by experiments in a standard geometry, the most common being the so-called "diameter-effect" experiment, which measures steady detonation velocity as a function of charge diameter in a "rate stick"—a long cylinder of explosive. The determination of  $D(\kappa)$  from these data is discussed in Ref. 5. We consider only  $-D'(\kappa) \geq 0$ .

The governing equations above are written in scaled variables; see Appendix A. In these variables, the Chapman-Jouguet (CJ) detonation velocity is unity, and the CJ reaction time is unity or at least  $O(1)$ .

For computation, the integral term in the coefficient  $B$  is split into two parts. We write it as

$$\int_0^\xi D\phi_\xi d\xi = \phi - \phi_e + \int_0^\xi (D-1)\phi_\xi d\xi \quad (3.3)$$

This has the advantage that the integral, which must be done numerically, is a small term, because  $(D-1)$  is the deviation of the (scaled) wave velocity from the CJ value of unity.

Another form of these equations is useful both for computation and analysis. We define a new angle variable  $u$

$$u = \phi - \theta \quad (3.4)$$

which has the nice property that  $u = 0$  at an edge to which the wave is normal. In this variable the governing equation is

$$u_t + Bu_\xi = -D'(\kappa)(u_{\xi\xi} + kS_\xi) - \theta'(t) \quad (3.5)$$

The added source term  $\theta'$  is the time derivative of the left edge angle  $\theta$  at the point at which the shock intersects the edge.

## (2) Boundary Conditions

For a free edge (vacuum) we ask whether the flow is supersonic or subsonic in the frame attached to the moving intersection point of the shock and the edge, i.e., whether the quantity  $(|\tilde{U}|^2 - C^2)$  at the shock, where  $\tilde{U}$  is the vector particle velocity in this frame and  $C$  is the sound speed, is greater than or less than zero. If the flow is supersonic, signals from the edge do not enter the explosive, and we apply no boundary condition. If the flow is subsonic, we force it to be sonic by setting the edge angle  $\sigma$  to the critical value, the value for which the flow is sonic. In effect, overall we bound  $\sigma$  from below by the critical value,  $\sigma_c$ . For the polytropic fluid equation-of-state (EOS) with finite, single-step reaction rate, the critical value of  $\sigma$  is given by

$$\tan \sigma_c = \sqrt{\frac{\gamma-1}{\gamma+1}} \quad (3.6)$$

For instantaneous reaction (a Huygens wave), the critical value is  $\sigma = 0$ .

In general, the total arclength  $\xi_2$  of the shock between the two edges is changing with time. For our numerical method we need this total arclength along the shock and its rate of change with time. This derivative is given by

$$\frac{d\xi_2}{dt} = B(\xi_2) - D_2 \tan \sigma_2 \quad , \quad (3.7)$$

where the subscript 2 denotes values at the right edge.

### (3) Transverse Acoustic Wave Speed

It is of some interest to know how fast an acoustic signal, for example, the head of an edge rarefaction, propagates into the explosive along the shock. The speed of a transverse wave along the shock is given by

$$\frac{d\xi_w}{dt} = (\pm\sqrt{C^2 - U^2} + B) \quad , \quad (3.8)$$

where  $\xi_w$  is the location of the wave head, +/- denotes a rarefaction originating at the left/right edge,  $C$  is the sound speed and  $U$  is the component of the particle velocity normal to the shock in the shock attached frame. The right-hand side (RHS) is evaluated on the explosive shock. For the polytropic fluid EOS, the first term is

$$\sqrt{C^2 - U^2} = D \sqrt{\frac{\gamma - 1}{\gamma + 1}} \quad . \quad (3.9)$$

The high frequencies associated with the acoustic wave head are not strictly compatible with a low-frequency theory like DSD. This is particularly an issue at early times. Consequently, there is some ambiguity associated with identifying a proper origin for the acoustic source,  $\xi_{w0}$ . Generally, select  $\xi_{w0}$  to be a short distance in from the physical edge. This protects the acoustic source from early-time, high-curvature DSD transients.

### (4) $D(\kappa)$ Functions

Qualitative changes in the shock propagation can occur for different  $D(\kappa)$  that satisfy  $-D'(\kappa) \geq 0$ . When  $D = 1 - \alpha\kappa$  with  $\alpha = \text{constant}$  for all  $0 \leq \kappa < \infty$ , then the shock passes over every point in the explosive. We use this simple model for the sample problems described in Chap. V.

Detonation in real explosives cannot be sustained in regions where  $\kappa > \kappa_f$  and where  $\kappa_f$ , the curvature at which detonation fails, is different for different explosives.

For example, not all the explosive detonates in the vicinity of a sharp corner. Near such features, the detonation shock does not extend into the corner but terminates at an interior point defined by  $\kappa = \kappa_f$ . The locus of all such points defines a virtual edge (interior to the physical edge). The explosive between the physical edge and the virtual edge fails to detonate; it does not undergo significant reaction on a relevant time scale. An example of a  $D(\kappa)$  function that can model this behavior is

$$D = D_f + (1 - D_f)\sqrt{1 - \kappa/\kappa_f} \quad , \quad (3.10)$$

where  $\kappa \leq \kappa_f$  and the failure velocity,  $D_f$ , satisfies  $0 < D_f < 1$ . A detonation failure model with these properties is described in Appendix B.

#### IV. INPUT AND OUTPUT

##### (1) Input

A sample input file is

```
'run'           'Onion'
'fluid'         3.0 0.0
'Dkap'         1 0.1           !alpha = 0.1
'geom'         1.0
'edgel'        1 -1.0 0.0 -1.57
'edger'        3 0.0 1.0 0.0
'xnet'         0.0 128 8.0
'tnet'         1.0 4 3.75
'ic'           2 -1.57 1.0 +1.0
'bcl'          3           !sonic
'bcr'          1           !no bc
'bcrt'         2           !soft right
'twav'         1 0.125     !twave (left bndry)
'ref1'         5 0.1       !Cyl. w/ linear D-kappa
'dials'        1.0 0.001 0.001
```

The general structure of the input line is keyword, option flag, data.

The run line is special. Not all lines have the option flag. For example, in the second line, fluid is the keyword; there is no option flag, and 3.0 and 0.0 are data items. In the third line, Dkap is the keyword; 1 is the option flag; and 0.1 is a data item. An exclamation mark designates the rest of the line as a comment. A line with an exclamation mark in column one is a comment line.

The only restriction on the order of the lines is that the run line must be present and must be the first line. Its string (Onion in the example) appears in headings on the output. The remaining lines can appear in any order; only those required for the problem at hand need be present.

---



---

**TABLE 4.1. INPUT DATA**

---

fluid	$\gamma, \delta^2$ $\gamma$ —polytropic-gas exponent $\delta^2$ —fraction of resolved heat release	Fluid properties
Dkap 1	$\alpha, \beta$ $\alpha$ —linear coefficient $\beta$ —bounding coefficient	D( $\kappa$ ) function Linear: $D = 1 - \frac{\alpha\kappa}{1+\beta\kappa}$
2	$\kappa_f, D_f, \sigma_f$ $\kappa_f$ —failure curvature $D_f$ —failure velocity $\sigma_f$ —failure wave spreading angle	Failure: $D = D_f + (1 - D_f)\sqrt{1 - \frac{\kappa}{\kappa_f}}$
3	$\kappa_f, D_f, \sigma_f$	Failure: $D = D_f + (1 - D_f)(1 - \frac{\kappa}{\kappa_f})$
geom	k k—(0=slab/1=cylinder)	Problem symmetry
xnet	$\xi_0, n, \xi_n$ $\xi_0$ —initial (left) $\xi$ n—number of intervals $\xi_n$ —final (right) $\xi$	Arclength net
tnet	$t_0, n, t_n$ $t_0$ —initial $t$ n—number of display intervals $t_n$ —final $t$	Time net

---



---

**TABLE 4.1. INPUT DATA (continued)**

ic		Initial Condition
1	$\phi$ $\phi$ - angle	Line
2	$\phi, r, s$ $\phi$ - initial angle $r$ - radius $s$ - sign ( $\phi_\xi$ )	Circle
3	$\phi, r, s$ , file dp10 dp10 - contains $\xi, \phi, \phi_\xi$	Data file
edgel, edger		Edge
1	$x, y, \theta, \xi_{em}$ $x, y$ - initial point $\theta$ - angle $\xi_{em}$ - edge arclength maximum	Line
2	$x, y, \theta, r, s, \xi_{em}$ $r$ - radius $s$ - sign of $d\theta/d\xi_e$	Circle
3	$x, y, \theta, \xi_{em}$ , files dp8/dp9 dp8/dp9 - contain list of $\xi_e$ and $\theta_e$ for (left/right) edge	Data file
bcl, bcr		Boundary conditions
1		No b.c.
2	$\sigma$ $\sigma$ - angle	Fixed angle $\sigma$
3	$\sigma_c, \xi_{et1}, \xi_{et2}, \sigma$ $\sigma_c$ - critical sonic angle $\xi_{eti}$ - edge arclength at b.c. transition points	Sonic, $\xi_e \geq \xi_{et1}$ No b.c., $\xi_{et2} \leq \xi_e < \xi_{et1}$ Fixed angle $\sigma$ , $\xi_e < \xi_{et2}$
4	$\xi_{et1}, \xi_{et2}, \sigma$	Huygens, $\xi_e \geq \xi_{et1}$ No b.c., $\xi_{et2} \leq \xi_e < \xi_{et1}$ Fixed angle $\sigma$ , $\xi_e < \xi_{et2}$



---



---

**TABLE 4.1. INPUT DATA (continued)**

---

bcrt		Right-boundary type
1		Hard
2		Soft
twav		Transverse wave
0		none
1	$\xi_{w0}, t_{w0}$	from left edge
2	$\xi_{w0}, t_{w0}$ $\xi_{w0}$ - source location $t_{w0}$ - initiation time	from right edge
ref1, ref2		Reference solution
1	$\alpha$ $\alpha$ - linear $D(\kappa)$ form	$D(\kappa)$ circle
2		Huygens circle
3		Huygens ramp corner
4		Huygens circ. corner
5	$\alpha$ $\alpha$ - linear $D(\kappa)$ form	$D(\kappa)$ circle
range		Plot ranges
1	$x_1, x_2, y_1, y_2$ $x_1, x_2$ - plot range of $x$ $y_1, y_2$ - plot range of $y$	Wave plot
dials		Dials
	$\Delta t/\Delta \xi, \text{delt}, \text{tol}$ $\Delta t/\Delta \xi$ - step ratio $\Delta t$ - integration time step delt - initial DPDES step tol - DPDES tolerance	

---



---

The input data specifications are summarized in Table 4.1. Detailed specifications for each line follow.

#### RUN - Run Label

The run label is the second string on the line. It appears in the output headings.

#### FLUID - Fluid Parameters

$$\begin{aligned} &\gamma, \delta^2 \\ &\gamma = \text{polytropic-gas exponent} \\ &\delta^2 = \text{fraction of resolved} \\ &\quad \text{energy release} \end{aligned}$$

The fluid equation-of-state is used in two places. It is used in calculating the sonic character of the flow at the edge in the sonic boundary condition, option 3 under bcl, bcr. It is also used in the separate calculation of the (transverse) speed of the head of the edge rarefaction wave along the shocks under twav.

The parameter  $\delta^2$  applies to the SRHR model (see Ref. 6). For this model, the sonic boundary condition depends on  $\delta^2$  and  $\gamma$ .

#### DKAP - $D(\kappa)$ Relation

1	$\alpha, \beta$ $\alpha, \beta$ - coefficients in $D = 1 - \alpha\kappa / (1 + \beta\kappa)$	Linear
---	--	--------

The  $D(\kappa)$  relation is linear, with coefficient  $\alpha$  for  $|\kappa|$  small, and  $D(\kappa)$  approaches  $1 - \alpha/\beta$  for  $\kappa$  large.

2	$\kappa_f, D_f, \sigma_f$ $\sigma_f$ - spreading angle $D_f, \kappa_f$ - coefficients in $D = D_f + (1 - D_f)\sqrt{1 - \kappa/\kappa_f}$	Failure Model A
---	---	-----------------

For Model A, detonation propagates only in regions where  $\kappa < \kappa_f$ . The detonation fails at  $\kappa = \kappa_f$ , with  $D'(\kappa_f) \rightarrow \infty$ . The spreading angle,  $\sigma_f$  of the failure wave along the shock is measured relative to the shock normal. See Appendix B for details.

3	$\kappa_f, D_f, \sigma_f$ $D_f, \kappa_f$ - coefficients in $D = D_f + (1 - D_f)(1 - \kappa/\kappa_f)$	Failure Model B
---	--	-----------------

Model B is similar to Model A above except that  $D(\kappa)$  is linear and  $D'(\kappa_f) = -(1 - D_f)/\kappa_f$ .

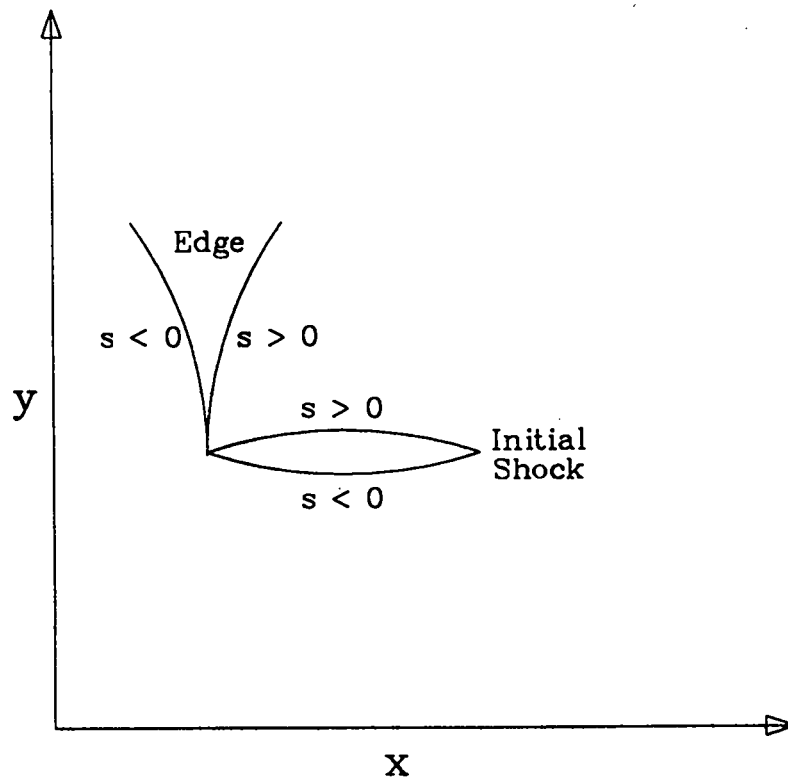


Fig. 4.1 Sign of  $s$  for the circular-arc edge ( $s = d\theta/d\xi_e$ ) and initial shock ( $s = d\phi/d\xi_e$ ).

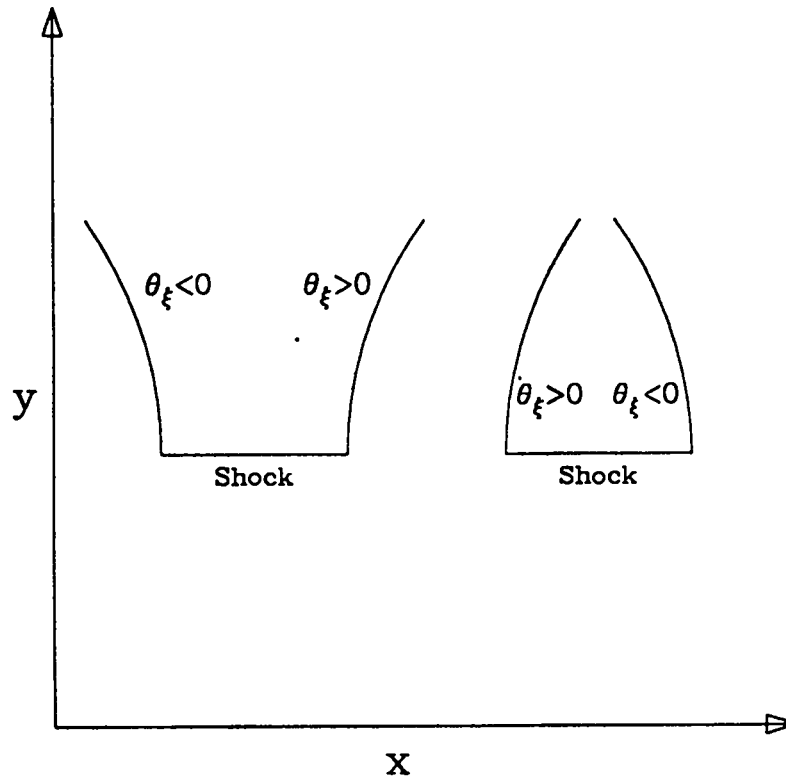


Fig. 4.2 Edges - circles

left:	$\theta = \theta_0 - \frac{\xi}{r}$	left:	$\theta = \theta_0 + \frac{\xi}{r}$
right:	$\theta = \theta_0 + \frac{\xi}{r}$	right:	$\theta = \theta_0 - \frac{\xi}{r}$

## GEOM - System Symmetry

$$k$$

$$k - (0 = \text{slab} / 1 = \text{cylinder})$$

For slab symmetry, the body is infinite in extent in the direction normal to the paper. For cylinder symmetry, the body is a figure of revolution about the  $x = 0$  centerline.

### IC - Initial Condition

1	$\phi$	Line
	$\phi$ - angle	

The initial shock is a straight line, which has inclination  $\phi$  at the left edge.

2	$\phi, r, s$	Circle
	$\phi$ - angle	
	$r$ - radius	
	$s$ - sign of $\phi_\xi$	

See Fig. 4.1. The initial shock is an arc of a circle of radius  $r$  and has inclination  $\phi$  at the left edge. The parameter  $s$  ( $\pm 1.0$ ) gives the sign of the curvature.

3	$\phi, r, s$	Data File
---	--------------	-----------

The input file is dp10. Its first three lines contain four data fields each. Of these, all but the first field in the first line (which contains the # points in the initial data) are dummy numeric fields. Lines 4 thru ( $3 + \# \text{ points}$ ) contain the triplets  $(\xi, \phi, \phi_\xi)$  that describe the initial shock shape. The file dp10 is written by the code at the final output time. It is used as initial data to solve problems with complex boundaries as a sequence of simpler problems.

# points	xx	xx	xx
xx	xx	xx	xx
xx	xx	xx	xx
$\xi$	$\phi$	$\phi_\xi$	

### EDGEL, EDGER - Left, Right Edge

1	$x, y, \theta, \xi_{em}$	Line
	$x, y$ - initial	
	$\theta$ - angle	
	$\xi_{em}$ - edge arclength maximum	

The edge is a straight line at angle  $\theta$  through  $(x,y)$ , the intersection of the edge with the initial shock.

2	$x, y, \theta, r, s, \xi_{em}$	Circle
	$r$ - radius	
	$s$ - sign of $d\theta/d\xi_e$	

See Fig. 4.2. The edge is a circular arc of radius  $r$ , total edge arclength  $\xi_{em}$ , initial angle  $\theta$ , through  $(x,y)$ , the point of intersection of the edge with the initial shock. The parameter  $s$  ( $\pm 1.0$ ) gives the sign of the curvature. A default value of  $\xi_{em}$  is used when no value (i.e., zero) is entered.

3	$x, y, \theta, \xi_{em}$ $\xi_e, \theta_e$ $\xi_e$ - edge arclength $\theta_e$ - angle of edge tangent	Data File
---	--	-----------

The input file is dp8/dp9 for the left/right edge. Its format is

# points  
 $\xi_e, \theta_e$

BCL, BCR - Left, Right Boundary Condition (b.c.)

1		No b.c.
---	--	---------

No boundary condition is to be applied. This is used at a supersonic edge.

2	$\sigma$ $\sigma$ - angle	Fixed angle $\sigma$
---	------------------------------	----------------------

The intersection angle  $\sigma$  between the shock's normal and edge tangent is to be fixed at the given value.

3	$\sigma_c, \xi_{et1}, \xi_{et2}, \sigma$ $\sigma_c$ - critical sonic angle $\xi_{eti}$ - edge arclength at b.c. transition points	Sonic, $\xi_e \geq \xi_{et1}$ No b.c., $\xi_{et2} \leq \xi_e < \xi_{et1}$ Fixed angle $\sigma$ , $\xi_e < \xi_{et2}$
---	--	---

The condition to be applied when  $\xi_e \geq \xi_{et1}$  is

If  $\mp \sigma > \sigma_c$ , no b.c. (supersonic)  
If  $\mp \sigma \leq \sigma_c$ ,  $\sigma = \sigma_c = \text{constant}$  (subsonic),

where  $\sigma_c > 0$  is the angle at which the flow at the edge is sonic, the (-) sign applies at the left boundary and the (+) sign at the right. If the flow at the edge is sonic or subsonic, make it sonic. No boundary condition is applied when  $\xi_{et2} \leq \xi_e < \xi_{et1}$ . When  $\xi_e < \xi_{et2}$ , the

intersection angle between the shock's normal and edge tangent is fixed at  $\sigma$ . The default value for  $\sigma_c$  is the polytropic gas expression,

$$\sigma_c = \arctan \sqrt{\frac{\gamma-1}{\gamma+1}} .$$

4	$\xi_{et1}, \xi_{et2}, \sigma$	Huygens, $\xi_e \geq \xi_{et1}$ No b.c., $\xi_{et2} \leq \xi_e < \xi_{et1}$ Fixed angle $\sigma$ , $\xi_e < \xi_{et2}$
---	--------------------------------	---

This is the prescription for the Huygen's solution, which is normal incidence. The algorithm is that described in 3 above, with  $\sigma_c = 0$ .

#### BCRT – Right Boundary Type

1	Hard
2	Soft

The “hard” right boundary applies the given right boundary condition (from the bcr line) at the right edge, lengthening or shortening the computation's  $\xi$ -length as required. For the “soft” right boundary the computational  $\xi$ -length is fixed; its right end does not in general coincide with the right edge. See Chap. VII in this report.

#### TWAV – Transverse Wave Flag

This option tracks the head of an acoustic wave along the DSD generated shock. The source of the disturbance is an edge rarefaction. For early times the head of this acoustic wave can lag the DSD calculation of the disturbed shock. This is because DSD is a long-wavelength theory.

0		No wave
1	$\xi_{w0}, t_{w0}$	Left-edge wave
2	$\xi_{w0}, t_{w0}$	Right-edge wave
	$\xi_{w0}$ – source location	
	$t_{w0}$ – initiation time	

Note: do not start the wave precisely at the edge.

#### REF1, REF2 – Reference Solutions

The reference solutions are displayed on the wave plot for comparison with the calculation; that specified by ref1 (linear  $D(\kappa)$ ) with a dashed line, and that specified by ref2 (Huygens) with a chain line.

1 or 5	$\alpha$	$D(\kappa)$ circle
2, 3, 4	$\alpha$ – from linear $D(\kappa)$ Huygens	$D = 1$ circle

The reference solution `ref1` is the exact solution for an expanding circular wave with  $D = 1 - \alpha\kappa$  (see Chap. VI). The solution `ref2` is a Huygens wave.

## DIALS - Integration Control

Equations (2.3), (3.1a), (3.1b), (3.7) and (3.8) control the evolution of the shock. The International Mathematical Software Library (IMSL) method of lines subroutine DPDES is used to integrate Eq. (3.1a). Equation (2.3) is integrated with a centered-difference scheme, while Eqs. (3.7) and (3.8) are integrated with a forward-difference scheme. The `xnet` line gives the initial mesh spacing along the shock ( $\Delta\xi = (\xi_n - \xi_0)/n$ ). The time step,  $\Delta t$  is entered indirectly through  $\Delta t/\Delta\xi$ . `Del t` is the initial DPDES time step and `tol` is the DPDES error tolerance.

## 2. Output

Terminal output is designed to monitor the progress of the calculations. A line is printed after each calculation step. Here `kt` is the number of the step, and `nxx` is the number of mesh points between the edges. For each edge the sonic character `son` (0/1 for sub/super), the boundary condition type `bdry` (1/2/3 for no b.c./fixed  $\sigma/\kappa = \kappa_f$ ), the detonation state `fail` (1/2 for detonating/failing) and the angle  $\sigma$  are shown. If the time is a display time, the letter "d" appears after the time. If this step involved a new DPDES start, the letter "n" appears after the value of `nxx`. The current DPDES time step `dph` and the total shock `arclength xi21` are also shown.

The printed output at each display time consists of one line containing the loop index `kt`, the time  $t$ , and edge quantities, and then the mesh print, consisting of one line for each mesh point, containing  $\xi$ ,  $\phi$ ,  $\phi_\xi$ ,  $D$ ,  $B$ ,  $x$ ,  $y$ , and  $x$  and  $y$  for each reference solution. This output is written to file `do`. In addition, the  $x$ ,  $y$  coordinates of the wavefront are written to `dp1` and the  $\xi$ ,  $\phi$  coordinates of the fronts are written to `dp5`.

The graphical output at the end consists of four plots: (1) the Fronts, showing the body, any failure loci, and successive shock shapes, (2) the wave angle  $\phi$  vs. arclength  $\xi$ , (3) the Phase Velocity  $D$  vs. time at the ends of the shock, and (4) the coefficient  $B$  vs. arclength  $\xi$ . Plots 1, 2, and 4 show one curve for each display time.

## V. SAMPLE PROBLEMS

We give the input data and results for several sample problems. The input files are given in Table 5.2. The output represents a selection; the complete output is not given for each problem. Data decks for a wide variety of sample problems are included at the end of the code. Instructions for running them can be found in Chap. VII of this report.

Problem 1 (data file `di1h` and Figures 5.1) is the Huygens solution for an expanding circle. The shock shapes at three times are shown in Fig. 5.1a. The left edge is a vertical

straight line, the right edge is a horizontal straight line, and the initial shock is a circle of unit radius. As specified by the 'Dkap' line of the input, linear  $D(\kappa)$  with  $\alpha = 0$  gives  $D = 1$  for the Huygens' solution. The left b.c. is that the wave be normal to the edge (the flow will always be sonic in this problem). The right boundary is a soft boundary, i.e., the right edge is the terminal locus for the display. The computation arclength remains fixed at its initial value of 4 ('xnet' line). Initially, the end point  $\xi_n = 4$  of the computation arc lies well beyond the right edge (which is at  $\xi = 1 \times (\pi/2)$  at the initial time  $t = 1$ ). To have the computation arc extend to the right edge up to time 4, we would have set  $\xi_n \geq 4 \times (\pi/2)$  (with a corresponding increase in computation time). The jagged line originating at the left boundary in Fig. 5.1a is the track of the acoustic wave head along the shock. It marks the leading edge along the shock of the rarefaction advancing from the left boundary. The roughness of the track gives a measure of the calculational mesh size. A total of 64 mesh points span the shock from  $\xi = 0$  to  $\xi = 4 \times (\pi/2)$ . The angle  $\phi$  vs.  $\xi$  for three times is shown in Fig. 5.1b. Table 5.1 shows the output written to the screen by this run.

Problem 2 (data file di1 and Figures 5.2) is the expanding circle for  $D = 1 - \alpha\kappa$ ,  $\alpha = 0.1$ . The geometry is the same as Problem 1. The left b.c. is  $\sigma = 0$  (normal incidence). The right b.c. is a soft boundary identical to the right boundary in Problem 1. The two reference solutions appear on the wave plot for comparison: (1) Huygens solution (chain dot line) and (2) exact solution (dashed line) (see Chap. VI of this report). The total number of mesh points is 64.

Problem 3 (data file di1p and Figures 5.3) is identical to Problem 2 with the exception that the number of mesh points is increased to 128. Comparing the results of these problems gives a measure of the sensitivity of our numerical algorithm to mesh size. The dependence on mesh size is weak. Also shown are the Huygens solution (chain dot line) and exact solution (dashed line).

Problem 4 (data file di2 and Figures 5.4) is similar to Problem 2 except that the sonic boundary condition is enforced along the left edge. It is a simple model of the onionskin experiment with the symmetry axis along  $y = 0$ . Note that along the left edge, the shocks shown in Fig. 5.4a curl back. The sonic boundary condition provides a model for an unconfined edge. A plot of the phase velocities in Figure 5.4c shows the velocity along the left edge (lower curve) is well below the velocity along the right edge (upper curve).

Problem 5 (data file di4c and Figures 5.5) considers a detonation with  $D = 1 - \alpha\kappa$ ,  $\alpha = 0.1$  propagating in a curved channel (arc shot). The geometry is cylindrical ( $k = 1$ ), with  $x = 0$  the axis of symmetry. The sonic boundary condition is applied along both edges. Figure 5.5b shows that the total shock arclength increases with time. As the right edge advances along the shock, Fig. 5.5c shows that the phase velocity increases there. Although the flow is originally sonic along this edge, after  $t = 3.5$  the flow becomes supersonic. The left edge pulls away from the shock. This leads to a phase velocity near 0.85 along this edge until late time when the convergence toward the symmetry axis accelerates the wave.

In problems 6 and 7 we consider an initially circular detonation propagating in an explosive whose geometry is shown in Fig. 5.6. These two problems (data files di6cb1, dp9 and di6cb2 and Figures 5.7-5.8) are designed to be solved sequentially. The sonic



boundary condition is applied along edges 1 and 3. Boundary 2 is a symmetry plane. In Problem 6 we consider the evolution of the shock up to the point when it just begins to encounter boundary 3. Using the final output from Problem 6 as initial data, in Problem 7 we follow the evolution of the shock as it advances along boundary 3. Figures 5.7 and 5.8a,b show the calculated shocks and the last portion of the shock phase velocity along edges 1 and 3. Problems with edge boundaries along which the boundary conditions change can be solved by either this sequential run strategy or by the segmented boundary option in bcl, bcr.

Appendix B. contains the solutions to some more complex problems.

---



---

**TABLE 5.1. OUTPUT FROM FILE di1**

---



---

```

21:59:05 05/27/92
dx di=di1
++ kt      t      nxr  son  bdry   fail   sig1   sig2   dph   xi21
++  1  1.0000d  26n  1 1  2  1   1  1  0.0000 -0.0083  0.0010  4.0000
++  2  1.0625   27  1 1  2  1   1  1  0.0000 -0.0911  0.0135  4.0000
++  3  1.1250   28  1 1  2  1   1  1  0.0000 -0.1096  0.0028  4.0000
++  4  1.1875   30  1 1  2  1   1  1  0.0000 -0.1270  0.0023  4.0000
++  5  1.2500   31  1 1  2  1   1  1  0.0000 -0.0921  0.0043  4.0000
++  6  1.3125   33  1 1  2  1   1  1  0.0000 -0.1092  0.0040  4.0000
++  7  1.3750   34  1 1  2  1   1  1  0.0000 -0.0784  0.0043  4.0000
++  8  1.4375   36  1 1  2  1   1  1  0.0000 -0.0951  0.0034  4.0000
++  9  1.5000d  37  1 1  2  1   1  1  0.0000 -0.0677  0.0071  4.0000
++ 10  1.5625   39  1 1  2  1   1  1  0.0000 -0.0841  0.0039  4.0000
++ 11  1.6250   40  1 1  2  1   1  1  0.0000 -0.0595  0.0025  4.0000
++ 12  1.6875   41  1 1  2  1   1  1  0.0000 -0.0753  0.0119  4.0000
++ 13  1.7500   43  1 1  2  1   1  1  0.0000 -0.0901  0.0071  4.0000
++ 14  1.8125   44  1 1  2  1   1  1  0.0000 -0.0683  0.0059  4.0000
++ 15  1.8750   46  1 1  2  1   1  1  0.0000 -0.0825  0.0112  4.0000
++ 16  1.9375   47  1 1  2  1   1  1  0.0000 -0.0624  0.0072  4.0000
++ 17  2.0000d  49  1 1  2  1   1  1  0.0000 -0.0762  0.0030  4.0000
plot done. pages = 5. words = 3527
graphics cl = u
END OF DISSPLA 10.0 -- 6756 VECTORS IN 4 PLOTS.
RUN ON 5/27/92 USING SERIAL NUMBER 433 AT LOS ALAMOS NATIONAL
LABORATORY
PROPRIETARY SOFTWARE PRODUCT OF ISSCO, SAN DIEGO, CALIF.
2737 VIRTUAL STORAGE REFERENCES; 6 READS; 0 WRITES.
end cft
dx      ctss time      16.960  seconds
cpu=    4.205 i/o=     8.285 mem=    4.471
prpp title="di1"

```

---



---

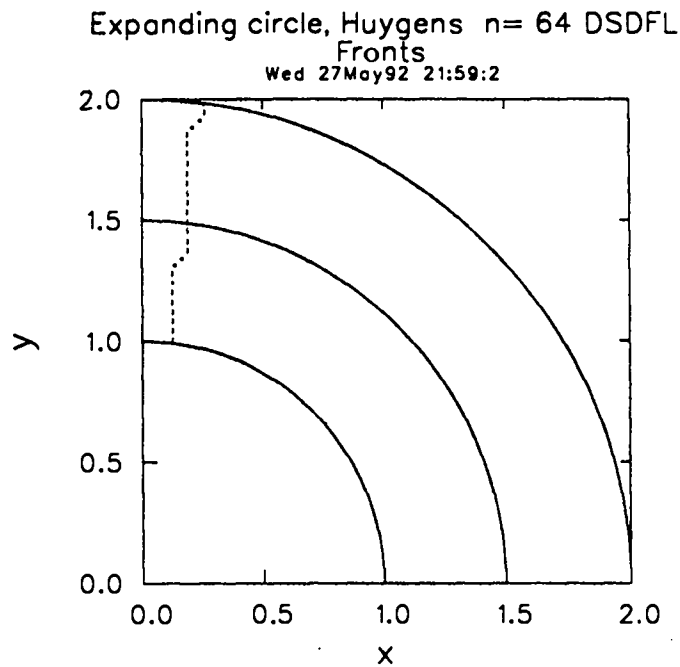


Fig. 5.1a Shock fronts for Problem 1 (file di1h). A circularly expanding Huygens wave with  $D = 1$ . The output times are  $t = 1$  (initial), 2 and 3. The jagged dashed line is the track of an acoustic wave along the shock (a radius vector for a Huygens wave).

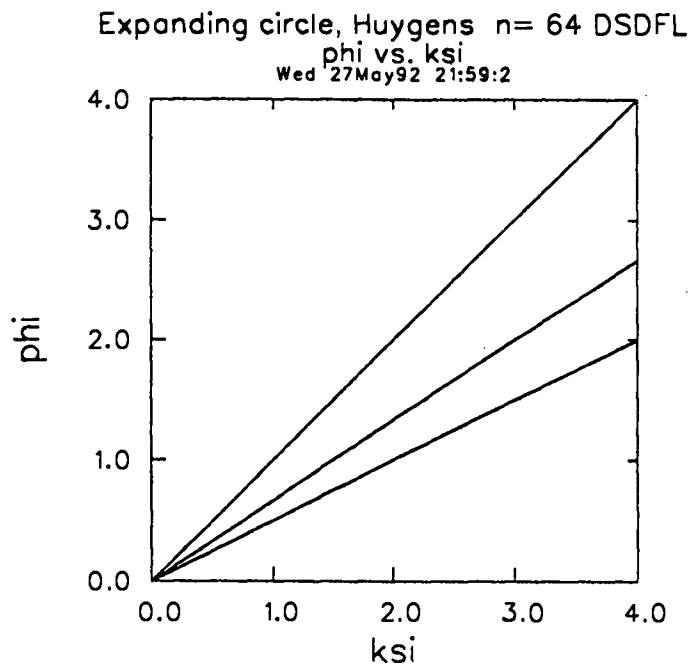


Fig. 5.1b  $\phi$  vs.  $\xi$  for Problem 1 (file di1h). The domain of interest is  $0 \leq \phi \leq \pi/2$ . The upper line corresponds to  $t = 1$  and the lower line to  $t = 3$ .

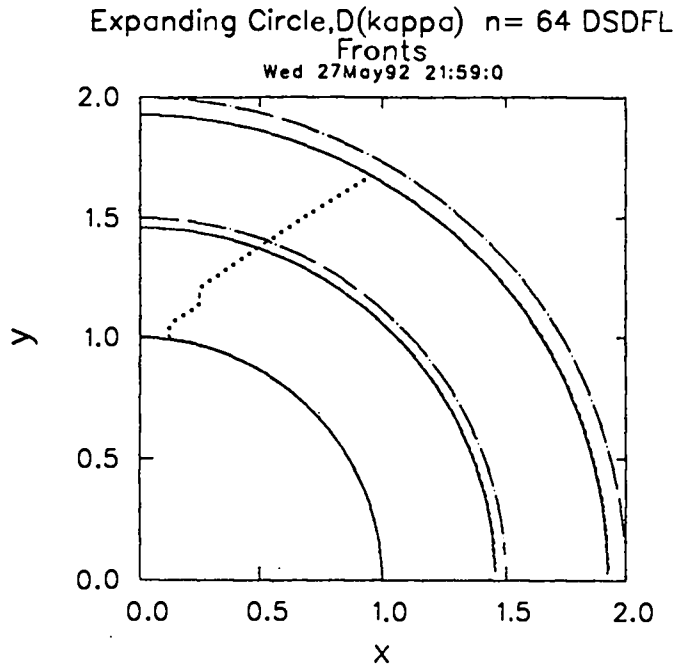


Fig. 5.2a Shock fronts for Problem 2 (file di1). A circularly expanding DSD wave with  $D = 1 - 0.1\kappa$ . The output times are  $t = 1$  (initial) 2 and 3. The solid line is the DSD wave, the chain dot line is the reference Huygens wave. The exact DSD wave (dash line) is just visible. Since the flow is subsonic along the shock, the acoustic wave head (jagged line) progresses inwards. The calculation uses 64 mesh points.

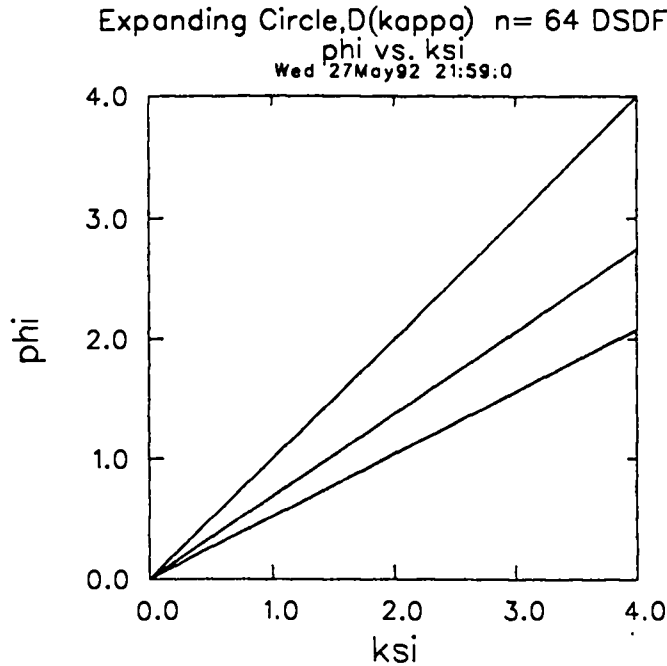


Fig. 5.2b  $\phi$  vs.  $\xi$  for Problem 2 (file di1).

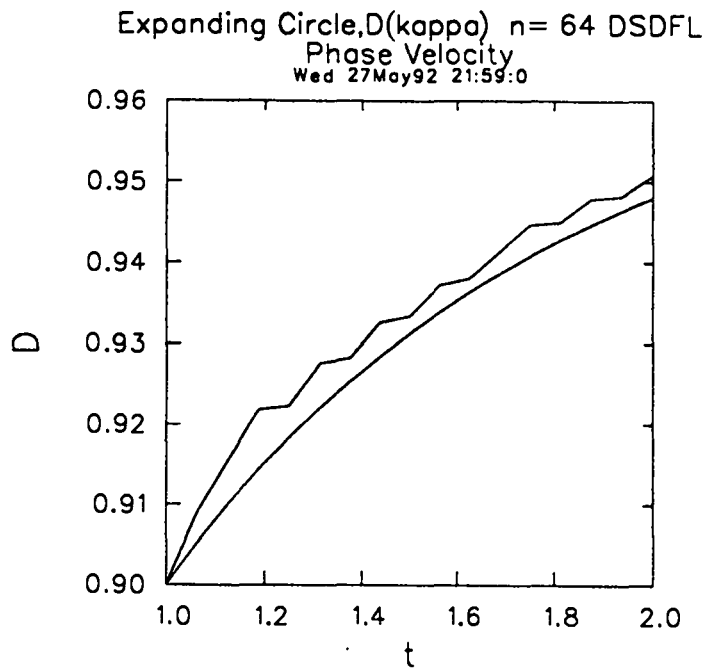


Fig. 5.2c Phase velocity at edges for Problem 2 (file di1). The jaggedness of the phase velocity along the right edge is a property of the soft right boundary (the right edge corresponds to  $y = 0$  and is not coincident with a mesh boundary).

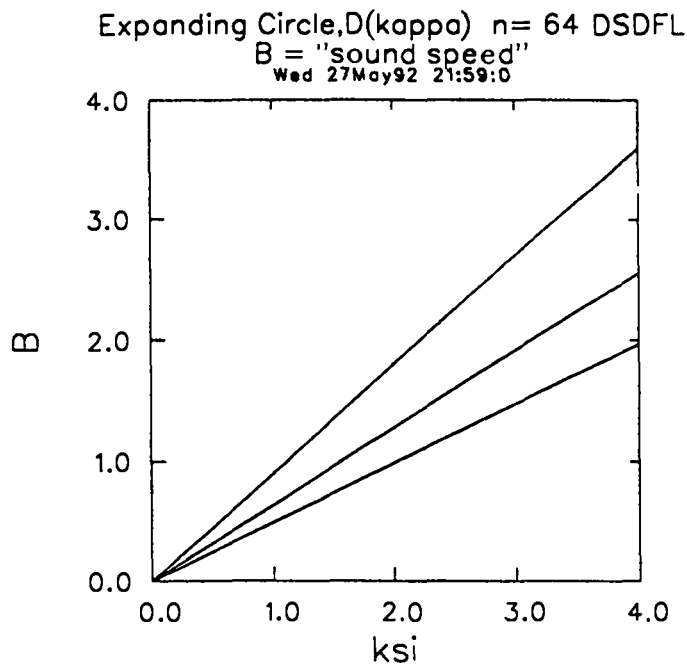


Fig. 5.2d The  $B$ -integral for Problem 2 (file di1).  $B$  corresponds to the speed with which a constant  $\phi$  feature moves along the shock when  $D$  is constant. By analogy with 1D gasdynamics, we call  $B = \text{"sound speed."}$

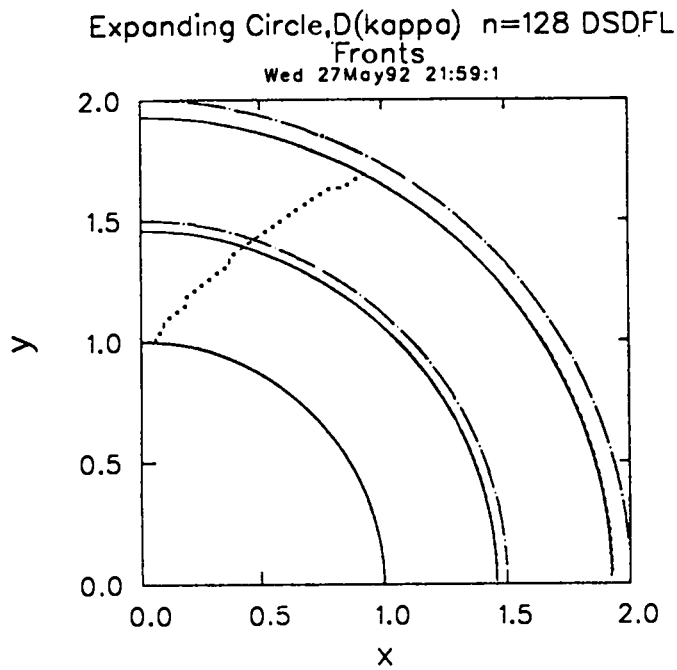


Fig. 5.3a Shock fronts for Problem 3 (file `di1p`). This problem is identical to Problem 2 except that 128 mesh points are used. The exact solution can no longer be seen, and the track of the transverse wave is smoother.

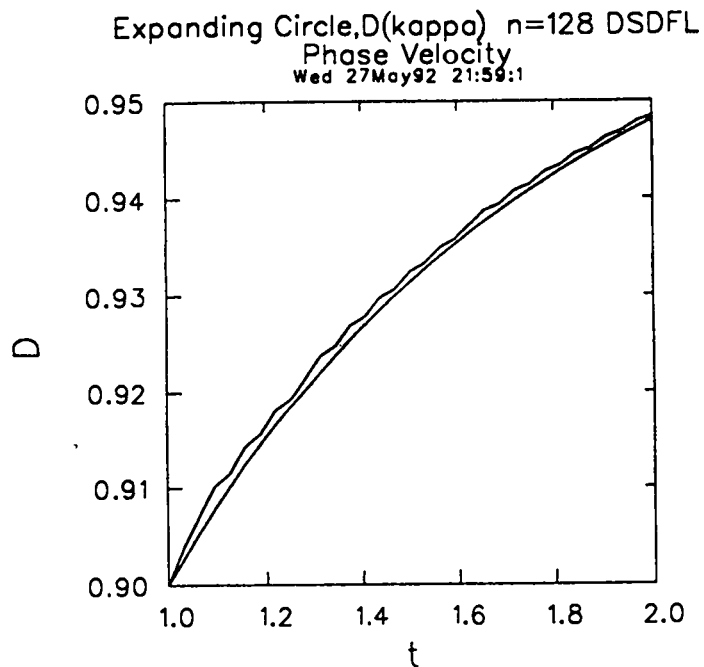


Fig. 5.3b Phase velocity at edges for Problem 3 (file `di1p`). The difference shown in Problem 2 between the phase velocity at the two edges is diminished.

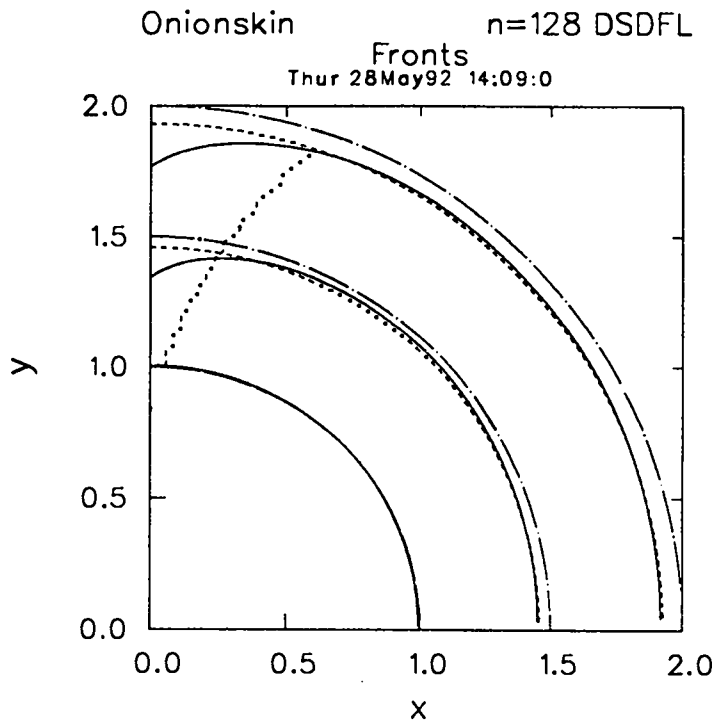


Fig. 5.4a Shock fronts for Problem 4 (file di2). A circularly expanding DSD wave with  $D = 1 - 0.1\kappa$ . The sonic boundary condition is applied along the left edge and  $y = 0$  is the symmetry axis. The output times and reference solutions are identical to those in Problem 2. The number of mesh points is 128 and the location of the acoustic source is 5 mesh points from the left edge. The dashed line corresponds to the exact solution when no disturbance enters at  $x = 0$ .

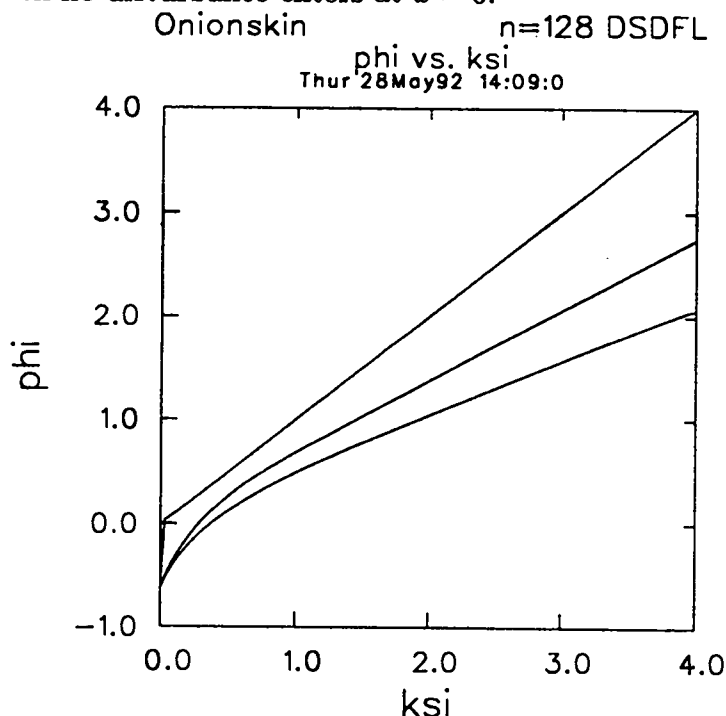


Fig. 5.4b  $\phi$  vs.  $\xi$  for Problem 4 (file di2).

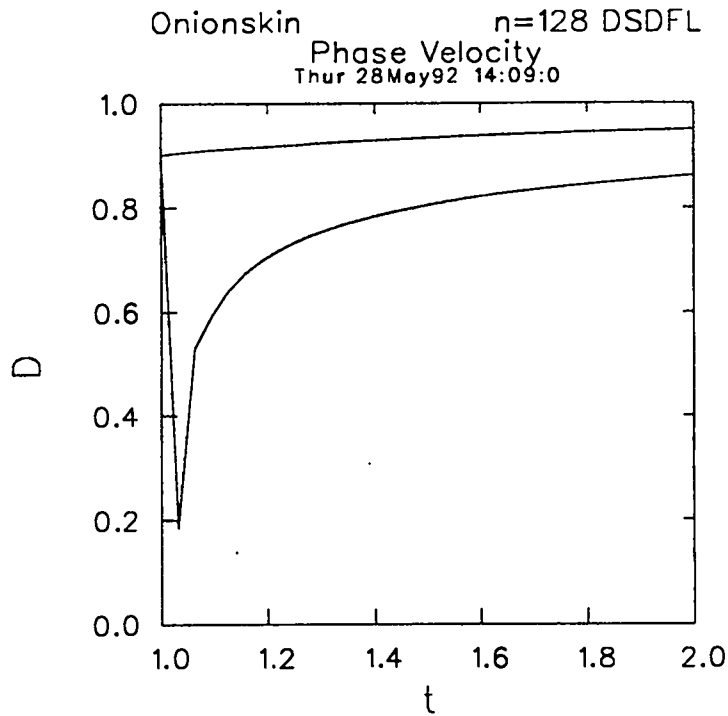
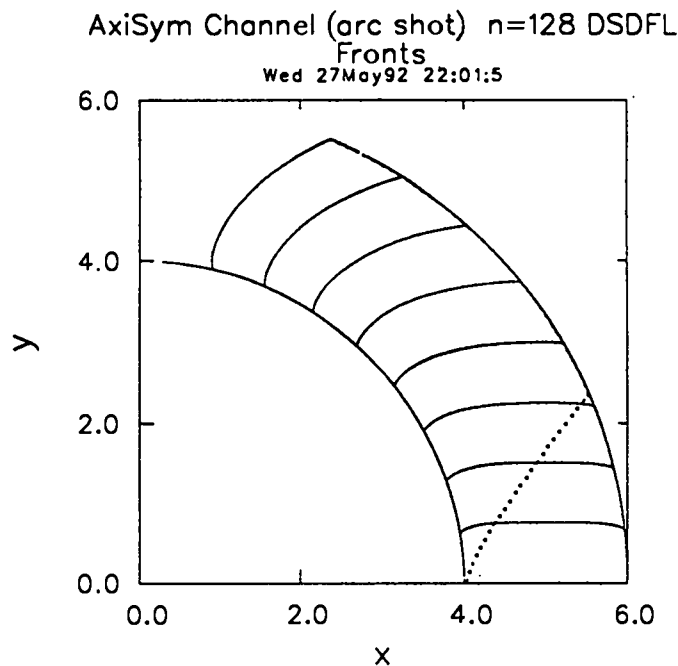


Fig. 5.4c Phase velocity at edges for Problem 4 (file di2). The phase velocity at the left edge (lower curve) shows the strong influence of the free edge. The proper short time transient is not captured by  $D = 1 - \alpha\kappa$ , since  $\kappa \rightarrow \infty$  at the edge at  $t = 0$ . However, the integrated effect of this artifact is small.



26 Fig. 5.5a Shock fronts for Problem 5 (file di4c). A DSD wave with  $D = 1 - 0.1\kappa$  propagates towards the axis in a spherical shell of explosive. The axis of symmetry is  $x = 0$  and the output times are separated by  $\Delta t = 0.75$ . The dashed line is the track of an acoustic wave that originates at the left edge.

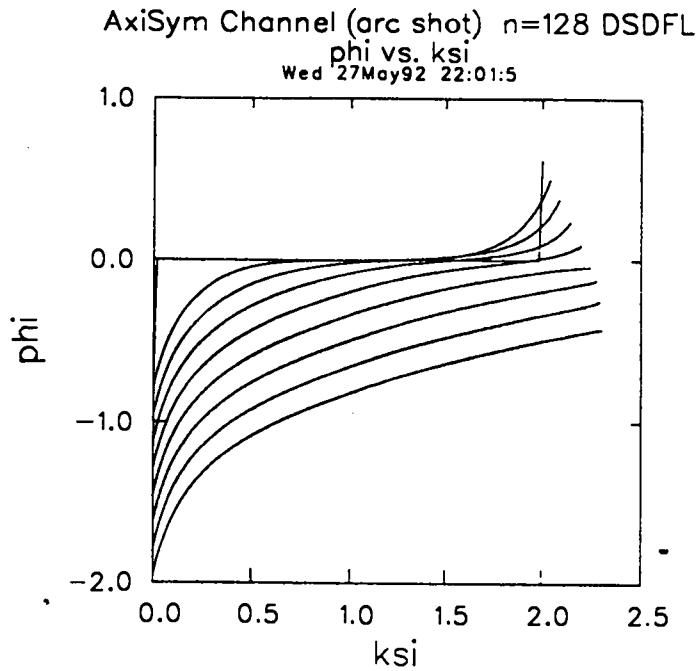


Fig. 5.5b  $\phi$  vs.  $\xi$  for Problem 5 (file di4c). As the shock propagates (lower curves are later in time) its total arclength increases.

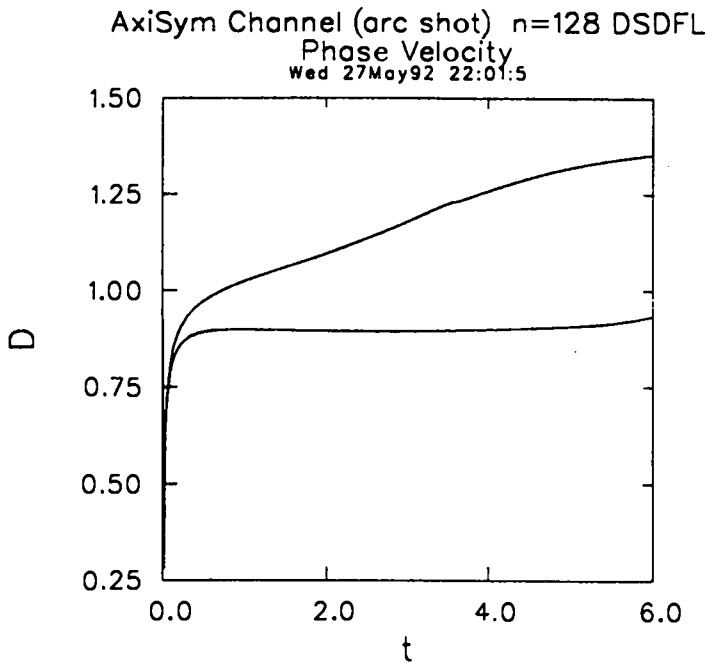


Fig. 5.5c Phase velocity at edges for Problem 5 (file di4c). The lower curve is the phase velocity along the left edge.



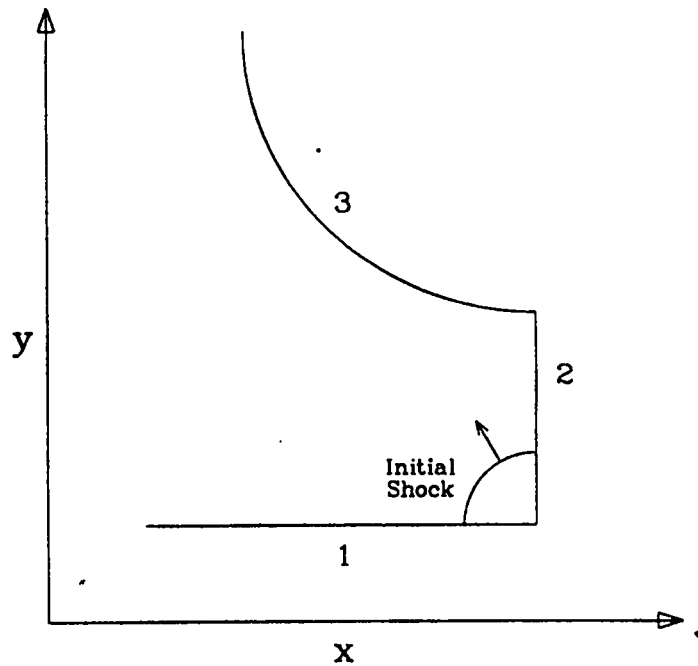


Fig. 5.6 The explosive geometry for Problems 6 and 7.

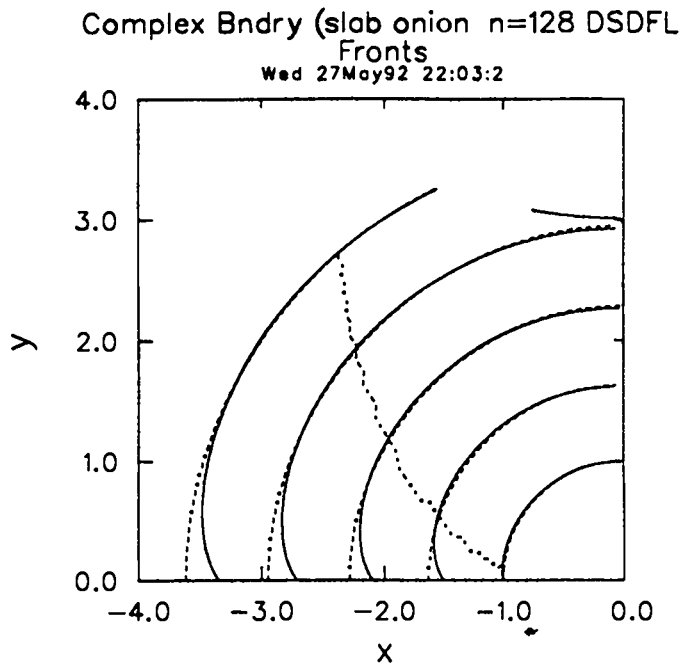


Fig. 5.7 Shock fronts for Problem 6 (files di6cb1 and dp9). A DSD wave with  $D = 1 - 0.1\kappa$  and a sonic boundary condition along the lower edge expands from a circular initial state. The symmetry line is  $x = 0$  and the dashed line corresponds to no edge effect along  $y = 0$ . The output times are separated by  $\Delta t = 0.6875$ .

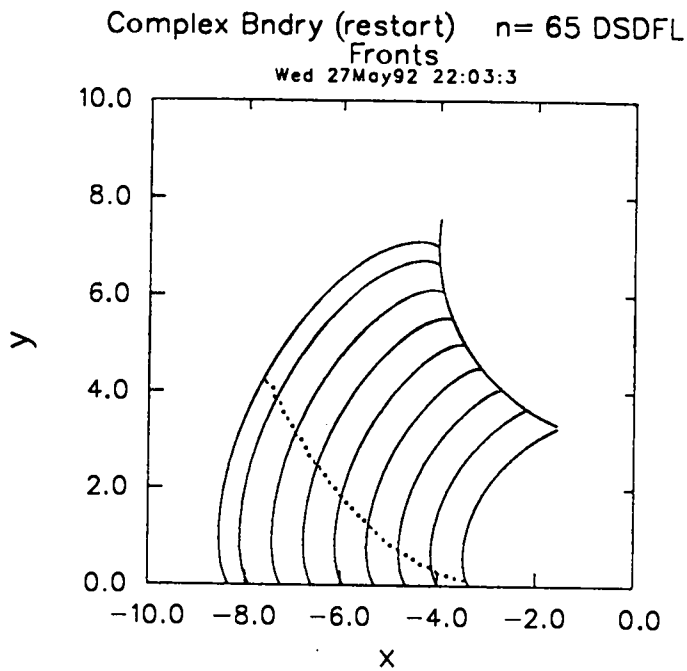


Fig. 5.8a Shock fronts for Problem 7 (file di6cb2). The output times are equally spaced except for the last shock.

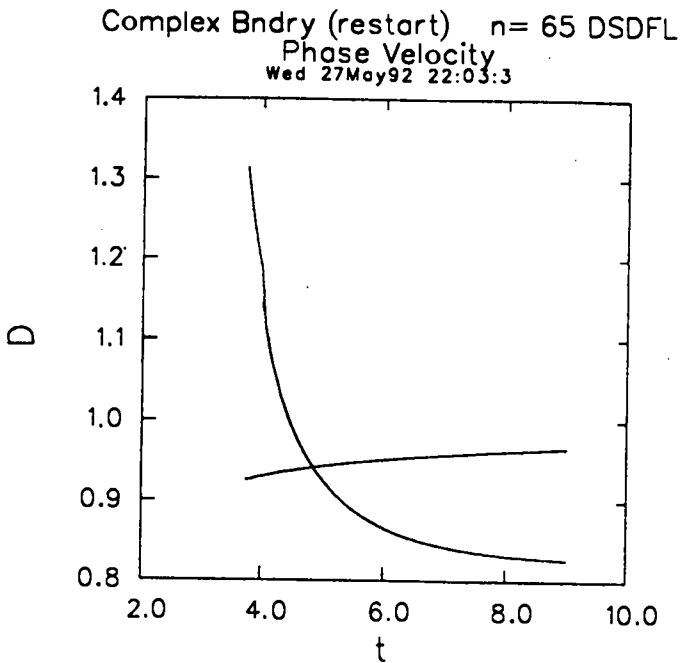


Fig. 5.8b Phase velocity at edges for Problem 7 (file di6cb2). Note how the phase velocity along the upper surface of the explosive (initially the upper curve) falls below 1 as the wave expands into the shadow zone.

---



---

**TABLE 5.2. INPUT FILES**

---

```

cat > dilh << "endcopytext"
'run'  'Expanding circle, Huygens'
!      Initial circle, soft right
'Dkap' 1 0.0          !CJ
'fluid' 3.0 0.0
'edgel' 1 0.0 1.0 0.0 !vert. line
'edger' 1 1.0 0.0 1.5708 !horiz. line
'xnet'  0.0 64 4.0
'tnet'  1.0 2 2.00
'ic'    2 0.0 1.0 +1.0
'bcl'   4          !Huygens
'bcr'   1          !no b.c.
'bcr't' 2          !soft right
'twav'  1 0.125    !twave(left bndry)
'range' 1 0.0 2.0, 0.0 2.0 !plot range
'ref1'   2          !Huygens D=1
'dials' 1.0 0.001 0.001

cat > dil << "endcopytext"
'run'  'Expanding Circle,D(kappa)'
!      Initial circle, soft right
'fluid' 3.0, 0.0
'Dkap'  1 0.1          !alpha = 0.1
'edgel' 1 0.0 1.0 0.0
'edger' 1 1.0 0.0 1.5708
'xnet'  0.0 64 4.0
'tnet'  1.0 2 2.00
'ic'    2 0.0 1.0 +1.0
'bcl'   2 0.0          !normal
'bcr'   1          !no bc
'bcr't' 2          !soft right
'twav'  1 0.125    !twave(left bndry)
'ref1'  1 0.1          !Cyl. w/ linear D-kappa
'ref2'  2          !Huygens D=1
'dials' 1.0 0.001 0.001

cat > dilp << "endcopytext"
'run'  'Expanding Circle,D(kappa)'
!      Initial circle, soft right
'fluid' 3.0, 0.0
'Dkap'  1 0.1          !alpha = 0.1
'edgel' 1 0.0 1.0 0.0
'edger' 1 1.0 0.0 1.5708
'xnet'  0.0 128 4.0
'tnet'  1.0 2 2.00
'ic'    2 0.0 1.0 +1.0
'bcl'   2 0.0          !normal
'bcr'   1          !no bc
'bcr't' 2          !soft right
'twav'  1 0.0625    !twave(left bndry)
'ref1'  1 0.1          !Cyl. w/ linear D-kappa
'ref2'  2          !Huygens D=1
'dials' 1.0 0.001 0.001

```

---



---

---



---

**TABLE 5.2. INPUT FILES (continued)**

---

```

cat > di2 << "endcopytext"
'run' 'Onionskin'
!      One free edge, initial circ., soft right
'fluid' 3.0, 0.0
'Dkap'  1 0.1          !alpha = 0.1
'edgel' 1 0.0 1.0 0.0
'edger' 1 1.0 0.0 1.5708
'xnet'  0.0 128 4.0
'tnet'  1.0 2 2.00
'ic'    2 0.0 1.0 +1.0
'bcl'   3          !sonic
'bcr'   1          !no b.c.
'bcrt'  2          !soft right
'twav'  1 0.0625    !twave(left bndry)
'refl'  1 0.1       !Cyl. w/ linear D-kappa
'ref2'  2          !Huygens D=1
'dials' 1.0 0.001 0.001

```

```

cat > di4c << "endcopytext"
'run' 'Axisym Channel (arc shot)'
!      Plane initial, hard right
'fluid' 3.0, 0.0
'Dkap'  1 0.05          !cj
'geom'  1.0
'edgel' 2 4.0 0.0 0.0 4.0 -1.0 !circle
'edger' 2 6.0 0.0 0.0 6.0 -1.0 !circle
'xnet'  0.0 128 2.0
'tnet'  0.0 8 6.00
'ic'    1 0.0          !line, theta = 0.0
'bcl'   3          !sonic
'bcr'   3          !sonic
'bcrt'  1          !hard
'twav'  1 0.03125     !twave(left bndry)
!'refl' 3          !cyl. diffract
'dials' 1.0 0.001 0.001

```

---



---

**TABLE 5.2. INPUT FILES (continued)**

---

```

! ----- Complex Bndry 1
cat > di6cb1 << "endcopytext"
'run' 'Complex Bndry (slab onion)'
! Circular initial data, soft right
'fluid' 3.0, 0.0
'Dkap' 1 0.1 ! alpha = 0.1
'edgel' 1 -1.0 0.0 -1.5708
'edger' 3 0.0 1.0 0.0
'xnet' 0.0 128 8.0
'tnet' 1.0 4 3.75
'ic' 2 -1.5708 1.0 +1.0
'bcl' 3 ! sonic
'bcr' 1 ! no bc
'bcrt' 2 ! soft right
'twav' 1 0.125 ! twave(left bndry)
'ref1' 5 0.1 ! Cyl. w/ linear D-kappa
!'ref2' 2 ! Huygens D=1
'dials' 1.0 0.001 0.001

```

```

! ----- file DP9 for DI6CB1
cat > dp9 << "endcopytext"
4
0.0, 0.0
1.999, 0.0
2.001, -1.5708
8.284, 0.0
endcopytext

```

```

! ----- Complex Bndry 2
cat > di6cb2 << "endcopytext"
'run' 'Complex Bndry (restart)'
! DI6CB1 output initial data, hard right
'fluid' 3.0, 0.0
'Dkap' 1 0.1 ! alpha = 0.1
'edgel' 1 -3.349 0.0 -1.5708 !line
'edger' 2 -1.564 3.326 -1.173 4.0 +1.0 !circle
'xnet' 0.0 65 4.0625
'tnet' 3.75 8 9.00
'ic' 3 -1.5708 3.675 +1.0
'bcl' 3 !sonic
'bcr' 3 !sonic
'bcrt' 1 !hard
'twav' 1 0.125 !twave(left bndry)
'range' 1 -10.0 0.0 0.0 10.0 !plot range
'dials' 1.0 0.001 0.001

```

## VI. EXACT SOLUTIONS

We give here a collection of exact solutions. There are several complete (time-dependent) solutions, mostly Huygens constructions, and some steady solutions.

### (1) Expanding Circle

For the expanding circular shock, the shock radius  $r(t)$  depends only on the time and the angle  $\phi$  (for a vertical reference edge) and is just  $\phi(\xi, t) = \xi/r(t)$ . For the curvature  $\kappa$  we have  $\kappa = \phi_\xi = 1/r(t)$ . For linear  $D(\kappa)$ , i.e.  $D = 1 - \alpha\kappa$ , we have

$$D = 1 - \alpha/r(t) \quad .$$

The kinematic equation, Eq. (3.1a) reduces to

$$dr/dt = D = 1 - \alpha/r(t) \quad .$$

The solution is

$$t(r) = r + \alpha \log \left( \frac{r - \alpha}{r_0 - \alpha} \right) \quad ,$$

where  $r_0(t_0) = t_0$  is the initial shock radius. For a given  $t$ ,  $r(t)$  may be found by iteration.

### (2) Huygens Construction

For Huygens construction, the DSD theory takes on an especially simple form. For the reader unfamiliar with the physics of our theory, a study of the following results will be well repaid. The equation for  $\phi$  is a simple kinematic-wave equation with a source term. If one is familiar with the type of hydrodynamics represented by this type of equation<sup>7</sup>, the nature of the solutions will be immediately apparent. The edge here plays the role of the "piston" of the usual formulation, and the solutions are simple waves.

The definition of a Huygens construction is

$$D = 1, \quad \sigma \geq 0.$$

That is, the shock velocity is everywhere the CJ velocity, and the shock makes an angle greater than or equal to  $\pi/2$  with the edge.

The  $D = 1$  condition makes the integral term in Eq. (3.3) and the RHS of the governing equation, Eq. (3.1a), vanish. When  $\sigma = 0$  (which we assume to be the case in these examples) the edge term  $D_e \tan \sigma$  in  $B$  is zero. It is most convenient to write the equations in the  $u$  variable of Chap. III of this report,

$$u = \phi - \theta \quad .$$

In this variable, the governing equations are particularly simple:

$$\begin{aligned} u_t + uu_\xi &= -\theta'(t) \\ \text{b.c. : } u &= 0 \text{ at } \xi = 0. \end{aligned}$$

The initial condition depends on the particular problem. In characteristic form we have

$$\frac{du}{dt} = -\theta'(t) \quad \text{on} \quad \frac{d\xi}{dt} = u \quad .$$

We consider three problems: (2a) circular expanding wave, (2b) channel with ramp edge, and (2c) channel with circular edge.

In 2a, the initial shock is a circle; in 2b and 2c, the initial shock is a straight line. The geometries are shown in Figs. 6.1, 6.2, and 6.3. For all three problems, there is no boundary condition at the right.

### (2a) Circular Expanding Wave

The left edge is a vertical line, that is  $\theta = 0$ . We have

$$\begin{aligned} u_t + uu_\xi &= 0 \\ \text{i.c. : } u &= \xi/r, \quad r = t_0 \text{ at } t = t_0 \quad . \end{aligned}$$

The initial shock is a circle of radius  $r = t_0$ , the assumption being that the wave began as a point at the origin at  $t = 0$ . The solution is analogous to the simple centered rarefaction of 1D gasdynamics

$$u = \frac{\xi}{t}, \quad \phi = \frac{\xi}{t} \quad .$$

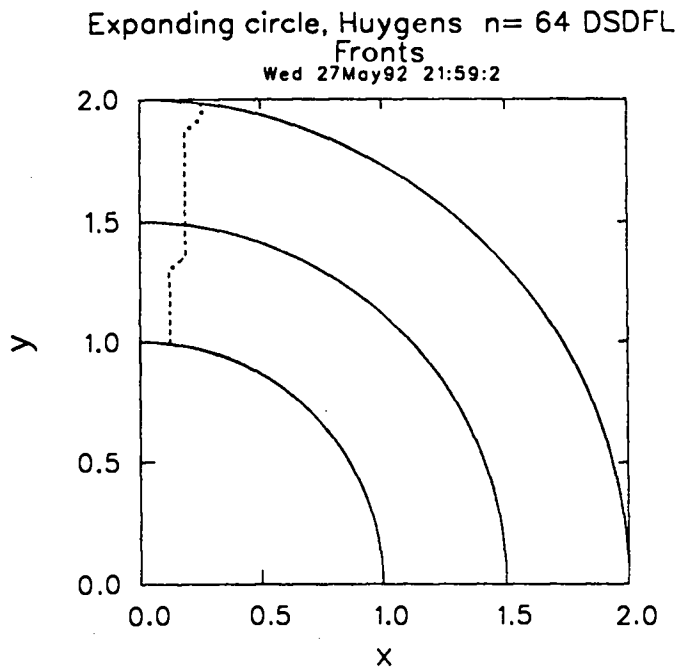


Fig. 6.1 Circular expanding Huygens wave.

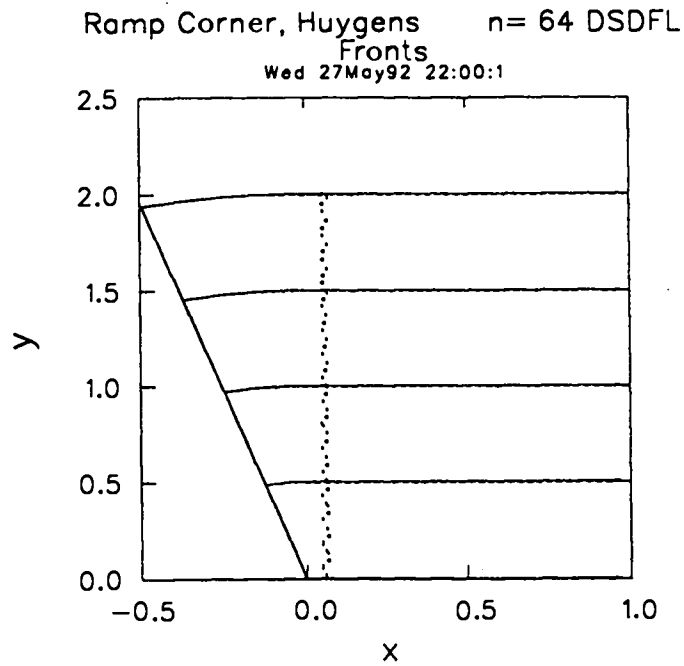


Fig. 6.2 Huygens wave for a channel with a ramp edge. Note the different  $x$  and  $y$  scales.



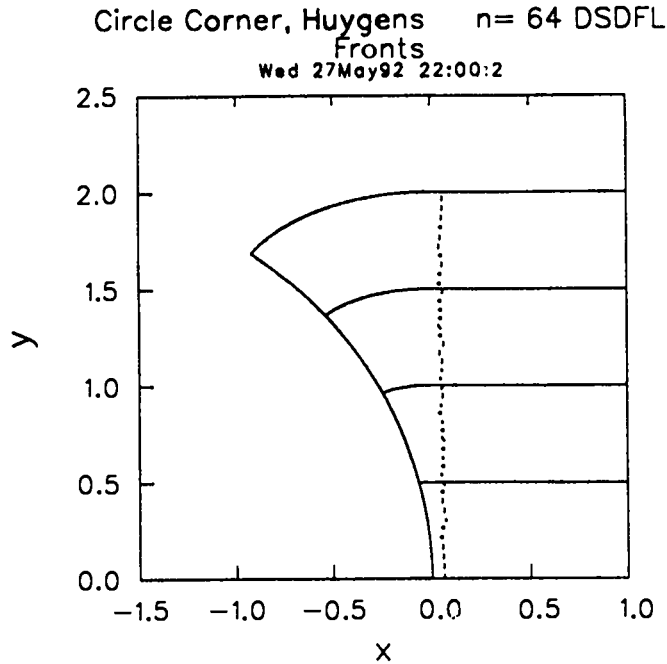


Fig. 6.3 Huygens wave for a channel with a circular edge.

The laboratory coordinates are

$$x = t \sin u$$

$$y = t \cos u .$$

(2b) Channel with Ramp Edge

We have  $\theta = \text{constant}$ ,  $\theta'(t) = 0$ ,  $\theta$  negative. The flat initial wave is the step function

$$\begin{aligned} u = 0 , & \quad \xi = 0 , \\ u = -\theta , & \quad \xi > 0 ; \end{aligned}$$

we must have  $u = 0$  at  $\xi = 0$  to match the edge. Again the solution is analogous to a simple centered rarefaction wave

$$\begin{aligned} u = \xi/t , & \quad \phi = \xi/t + \theta , & \quad \xi < -\theta t , \\ u = -\theta , & \quad \phi = 0 , & \quad \xi \geq -\theta t . \end{aligned}$$

The laboratory coordinates are

$$\begin{aligned}
 x &= t \sin \phi , & \xi < -\theta t \\
 &= \xi + \theta t , & \xi \geq -\theta t \\
 y &= t \cos \phi , & \xi < -\theta t \\
 &= t , & \xi \geq -\theta t .
 \end{aligned}$$

(2c) Channel with Circular Edge

We take a flat initial wave, with the left boundary a circle of radius  $r$ . The center of the circle is at  $x = -r, y = 0$ , so that  $\theta_0 = 0$ . The angle  $\theta$  is a linear function of time

$$\theta = -t/r ,$$

$$\theta'(t) = -1/r .$$

The governing equation is

$$u_t + uu_\xi = 1/r ,$$

$$\text{i. c. : } u = 0 \text{ at } t = 0 .$$

As in Problem 2b, we have the analog of a 1D rarefaction wave moving into a constant state, this time noncentered because of the gradual pulling away of the boundary. The characteristics are parabolas. The characteristic  $\xi = t^2/2r$  through the origin is the head of the rarefaction wave. The solution is

$$u = \sqrt{2\xi/r} , \quad \phi = \sqrt{2\xi/r} - t/r , \quad \xi \leq t^2/2r ,$$

$$u = t/r , \quad \phi = 0 , \quad \xi \geq t^2/2r .$$

The laboratory coordinates of the wave front are

$$x = r[(su + c) \cos u + (cu - s) \sin u - 1] ,$$

$$y = r[(cu - s) \cos u - (su + c) \sin u] ,$$

$$c \equiv \cos \theta , \quad s \equiv \sin \theta , \quad \theta = -t/r .$$

## VII. CODE STRUCTURE

In this chapter, we describe the internal structure of the code itself. We begin by outlining the main features of the numerical solution of the governing equations contained in the FORTRAN source code. Next we describe the FCL control file, the main loop of the program, and finally various pieces and subsystems of the program.

### (1) The Numerical Solution

The governing equation, Eq. (3.1) is in general a parabolic PDE. To solve it, we use the International Mathematical Software Library (IMSL) routine DPDES. For a  $\xi$ -net with  $n$  intervals, DPDES converts the PDE into a set of ODE's, which it solves with a version of the Gear<sup>8</sup> method. In each interval, the function  $\phi(\xi)$  is fit with a cubic Hermite polynomial with time-dependent coefficients. The coefficients are constrained by the requirement that the function and its first derivative must be continuous at the ends of the interval (i.e., at the knots). These coefficients are the solution of the ODE's. If  $n$  is the specified number of intervals in  $\xi$  (as given in our 'xnet' line), there are  $2n + 2$  ODE's, two between each knot and one at each boundary. The DPDES recipe evaluates the PDE at two Gaussian points per  $\xi$  interval to get the two collocation ODE's for each interval. The boundary conditions replace the PDE at the two edges of the domain.

Let us first define some terms. We use the term *time step* to mean the time step covered by one call of DPDES. For each call, one specifies two times ( $t_1$  and  $t_2$ ), and asks DPDES to integrate from  $t_1$  to  $t_2$ . In doing so, DPDES usually chooses several smaller internal time steps of its own to satisfy the specified error tolerance. Ordinarily, we are not concerned with these, but when we are, we will refer to them as *DPDES internal time steps*. The time step  $\Delta t$  is calculated from the space step  $\Delta \xi$ . Its value is such that the ratio  $\Delta t / \Delta \xi$  is approximately equal to the value of the first item, *xtrat*, on the *dials* line, for which we ordinarily take the value one. Decreasing *xtrat* improves the solution quality for problems with curved boundaries and/or large changes in total shock arclength. The penalty incurred in increased computation time is modest. For some problems the DPDES time integration error tolerance, *tol*, needs to be decreased in order to maintain solution symmetry. These improvements can be costly.

For our application, the two main shortcomings of DPDES are: (1) it has no way of evaluating the integral over  $\xi$  in the *B* term of Eq. (3.1), and (2) it can apply a boundary condition only at fixed  $\xi$ .

We handle the *B*-coefficient integral as follows: Before each time step we have  $\phi$  and  $\phi_\xi$  at each  $\xi$ , supplied by DPDES from the previous step. We calculate  $D(\xi)$ ; we now have all we need for the integrand. We then use a spline integration routine to calculate the value of the integral at each  $\xi$ . It remains constant at this value throughout the next DPDES step.

For most problems that we do, the total arclength along the shock changes with time. In order to use DPDES efficiently at any instant of time, we transform to a constant length

coordinate

$$z \equiv (\xi - \xi_0)(\xi_2(0) - \xi_0) / (\xi_2(t) - \xi_0) \quad ,$$

in place of  $\xi$ , where  $\xi_2(t)$  is the total arclength along the shock given by Eq. (3.7). Using  $t, z$  as the independent variables, Eq. (3.1a) becomes

$$\phi_t + \frac{(\xi_2(0) - \xi_0)}{(\xi_2(t) - \xi_0)} \left( B - \frac{z}{(\xi_2(0) - \xi_0)} \frac{d\xi_2(t)}{dt} \right) \phi_z = - \frac{(\xi_2(0) - \xi_0)}{(\xi_2(t) - \xi_0)} D_z \quad , \quad (7.1)$$

while the B-integral, Eq. (3.1b) maintains the same form with  $dz$  replacing  $d\xi$ . In these coordinates, both edge boundaries are at fixed  $z$  locations:  $z = 0$  and  $z = \xi_2(0) - \xi_0$ .

## (2) FCL Control

The source file DSD is an FCL control file. Both CTSS and UNICOS versions are available.

### Typing

```
fcl dsd
```

will cause the file to compile itself and produce an executable file dx.

In outline, the DSD file has the following form

FCL prologue

HISTORIAN call

DSD - program source code

Documentation

Input files

Compile and load

Many of the variables of the code are in common; we use HISTORIAN to place a copy of the common blocks in each routine. The documentation and input-file sections are described below. The compile and load commands are the standard ones.

At the end of the file is a documentation section, enclosed in `copytext nul /endcopytext` lines. This contains the conventions used for choosing variable and routine names and lists of all the variable and routine names and their meanings. Following the documentation section is a collection of input files, each enclosed in a pair of lines like `copytext di1 /endcopytext`. Thus execution of DSD under FCL produces a number of input files `di1, di2, . . .`. To execute dx with input file `di1`, type

$$dx \quad di = di1 \quad .$$

The DSD code uses the following libraries:

SUBL – private library containing utilities and DPDES

CLAMS – LANL math library

DISSPLA – proprietary graphics package.

### (3) Main Loop

The main loop is in routine `dsd`. Before the loop begins, `init` and `ic` are called. The subroutine `init` calculates derived constants and initializes counts. The initial shock and the edges are set up in `ic`.

The loop index `kt` goes from 1 to `nt`, the number of computation steps. Computation routines `step` and `stepf` are called in the loop. The subroutine `step` advances from the current time to the next by calling DPDES and then advances other things, such as the edge  $\theta$ 's, by centered forward difference. The coefficients needed by Eq. (7.1) for the next time step are calculated in `step` and any intersection of the real and virtual edges is determined there. The subroutine `stepf` sets the boundary conditions and calculates things after the step, such as the shock velocity and the  $B$ -integral. The first time through the loop, with `kt=1`, `step` is skipped; thus `stepf` does its calculation on the initial data.

The main output routines are `out` and `outf`. The subroutine `out` is called in the loop at display times. It prints the mesh, and then writes quantities from it on files for graphical display at the end. The subroutine `outf`, called after the loop is complete, does all the graphical display, getting the mesh quantities from the files written by `out`. The small routine `outp`, called at each computation step, saves quantities from each "path," such as the transverse-wave tracks, for display at the end by `outf`.

### (4) Edges

The edge quantities are stored in two-dimensional arrays, with index  $j = 1, 2$  for the left and right. The edge calculations are done in loops  $j = 1, 2$ .

Function routines `edge( $\xi_e, j$ )` furnishes the angle  $\theta$  for edge  $j$  from the current edge arclength  $\xi_e$ . In `ic`, equally spaced arclengths  $\xi_e$  along the edge are generated and stored in an array. The function `edge` is then called for each entry to generate a corresponding  $\theta(\xi_e)$ . Then `lab` is called to calculate arrays of laboratory edge coordinates  $x$  and  $y$  from  $\theta$  and  $\xi_e$ , from Eqs. (2.4). (In the output wave diagram, the edges are plotted from these arrays.) Spline-fit coefficients for  $x(\xi_e)$  and  $y(\xi_e)$  are then obtained from `spfit` for later

use in stepf.

In step the current edge arclength  $\xi_e$  is advanced using the mean phase velocity  $D_{ph}$

$$\xi_e = \xi_e + D_{ph} * dt \quad ,$$

where  $D_{ph}$  is the mean phase velocity from the old and new times. The current shock arclength,  $\xi_2(t)$ , is advanced using the current value of the B-integral

$$\xi_2 = \xi_2 + (B(\xi_2) - D_2 \tan \sigma_2) * dt \quad .$$

In stepf, the spline routine `spval` is used to calculate the current edge laboratory coordinates  $x$  and  $y$  from the edge arrays  $x(\xi_e)$  and  $y(\xi_e)$ , using the spline coefficients generated in `ic`. These values of  $x$  and  $y$  at the left are needed to get the shock  $x$  and  $y$  from Eq. (2.1). The boundary conditions for the next time step are set in stepf.

#### (5) Time Step

The `tnet` input data are  $t_0$ ,  $n_d$ ,  $t_n$ , the initial and final times  $t_0$  and  $t_n$  and the number of display times  $n_d$ . In `init`, the computation time step  $\Delta t$  is set to the step-ratio parameter (nominally unity) item from the dial input line times the space step  $\Delta \xi$ . The number of time steps is the next larger integer of  $(t_n - t_0) / \Delta t$ . An integer compute-display ratio, the next larger integer of  $(\Delta t / n_d)$ , is used in the main loop to decide when to call the output routine out.

## REFERENCES

1. J. B. Bdzil and D. S. Stewart, *Phys. Fluids A.* **1**, 1261-1267 (1989).
2. J. B. Bdzil, W. Fickett, and D. S. Stewart, "Detonation Shock Dynamics: A New Approach To Modeling Multi-Dimensional Detonation Waves," in Proceedings of The Ninth Symposium (International) on Detonation, Portland, OR, August 28-September 1 1989, pp. 730-742.
3. G. B. Whitham, Linear and Nonlinear Waves (Wiley, New York, 1974).
4. B. D. Lambourn and D. C. Swift, "Application Of Whitham's Shock Dynamics Theory To The Propagation Of Divergent Detonation Waves," in Proceedings of The Ninth Symposium (International) on Detonation, Portland, OR, August 28-September 1 1989, pp. 784-797.
5. J. Lee, P-A. Persson, and J. B. Bdzil, "Detonation Shock Dynamics of Composite Energetic Materials," *Phys. Fluids A.*, submitted, 1991.
6. J. B. Bdzil and D. S. Stewart, *J. Fluid Mech.* Vol. 171, 1-26 (1986).
7. W. Fickett, Introduction to Detonation Theory (University of California Press, Berkeley, 1985).
8. C. W. Gear, Numerical Initial Value Problems in Ordinary Differential Equations (Prentice-Hall, Englewood Cliffs, 1971).
9. D. S. Stewart and J. B. Bdzil, *Combustion and Flame* Vol. 72, 311-323 (1986).
10. R. Klein and D. S. Stewart, "The Relation Between Curvature, Rate State-Dependence and Detonation Velocity," submitted, *SIAM J. Appl. Math.* (1992).

## Appendix A. SCALING

Outside of this appendix we use scaled variables for which the CJ detonation velocity is unity and the CJ reaction time and length are unity or at least  $O(1)$ . In this appendix only, we use plain symbols for physical (dimensional) quantities and barred symbols for scaled variables. Then we drop the bars for the rest of the report. To most simply illustrate the scaling, we take the  $k = 0$  case (slab symmetry).

The governing equation, Eq. (3.1) is

$$\begin{aligned}\phi_t + B\phi_\xi &= -D'(\kappa)\phi_{\xi\xi} \\ B &= \int_0^\xi D\phi_\xi d\xi + D_e \tan \sigma \quad ,\end{aligned}\tag{A.1}$$

where  $\kappa = \phi_\xi$ . A typical  $D(\kappa)$  relation is the linear form

$$D = D_{CJ}(1 - \alpha\kappa) \quad .\tag{A.2}$$

Letting  $\mathcal{L}$  and  $t$  be length and time, and using square brackets to denote "dimension of," we have for the main dimensioned quantities

$$\begin{aligned}[D] &= \mathcal{L}/t \quad , \\ [\kappa \equiv \phi_\xi] &= 1/\mathcal{L} \quad , \\ [B] &= \mathcal{L}/t \quad , \\ [\alpha] &= \mathcal{L} \quad .\end{aligned}\tag{A.3}$$

For time, velocity, and distance scales, we take

$$\begin{aligned}t^* &= 1/Z \quad , \\ D^* &= D_{CJ} \quad , \\ \xi^* &= D^*t^* \quad ,\end{aligned}\tag{A.4}$$

where  $Z$  is the reaction-rate multiplier. We assume that  $Z$  is such that the CJ reaction time is  $Z^{-1}$  or at least  $O(Z^{-1})$ . We define scaled variables



$$\begin{aligned}
\bar{t} &= t/t^* \quad , \\
\bar{\xi} &= \xi/\xi^* \quad , \\
\bar{D} &= D/D^* \quad , \\
\bar{\kappa} &= \xi^* \kappa \quad , \\
\bar{\alpha} &= \alpha/\xi^* \quad .
\end{aligned}
\tag{A.5}$$

Applying these transformations, and dropping the bars gives Eq. (3.1) and

$$D = 1 - \alpha \kappa$$

for the linear  $D(\kappa)$  relation.

## Appendix B. DETONATION FAILURE MODELS

A limited amount of theoretical work<sup>6,9</sup> exists to support the idea that  $D(\kappa)$  is the propagation law for weakly curved, diverging detonation shocks. The object of these studies was to examine how simple detonation models respond to weakly two-dimensional perturbations of wavelength much longer than the reaction-zone length<sup>10</sup>. They show that if  $\kappa$  is sufficiently small,  $D(\kappa)$  describes the response of the shock to such perturbations. This is true even for explosives whose heat-release rates are moderately sensitive to the local state. These calculations do not show detonation extinction. Our development of the DSD model of detonation propagation was motivated by these results.

All real explosives exhibit detonation failure. For a number of important explosives (e.g., ammonium nitrate and fuel oil emulsion explosives and the triamino-trinitrobenzene (TATB) explosive PBX9502), it is observed that detonation is extinguished when the radius of curvature of the shock exceeds a critical value<sup>5</sup>. For these important materials, the detonation shock is smooth and broadly curved up to the onset of extinction. We interpret these observations as showing that  $D$  is a function of  $\kappa$  for these materials even when the interaction between  $\kappa$  and the state-dependence of the explosives' heat-release rate becomes large enough to produce extinction. Based largely on these experimental observations and with no theoretical support, we have extended our numerical algorithm to treat extinction.

### (1) The Failure Model

The detonation failure model has two additional parameters: (1) a critical or failure curvature,  $\kappa_f$  and (2) the spreading angle,  $\sigma_f$  measured relative to the shock normal, of the failure wave along the shock. Consult Fig. 2.3 for a definition of the various angles. Our extinction model consists of the following six components:

- (1) detonation is sustainable only where  $\kappa < \kappa_f$ ,
- (2)  $\kappa$  first exceeds  $\kappa_f$  on the physical boundary (edge), in response to abrupt changes in either b.c. type or edge shape,
- (3) the current b.c. on  $\phi_e$  (i.e., one of the standard set of b.c.) is replaced by a b.c. on the curvature,  $\kappa = \kappa_f$  when as described in (2)  $\kappa \geq \kappa_f$ ,
- (4) if at the onset of failure  $\sigma < \sigma_f$ , then the failure wave propagates into the explosive and generates a virtual edge separating "dead" explosive from detonating explosive. This boundary is defined by  $\theta = \phi_e - \sigma_f$ , where  $\kappa = \kappa_f$  is the boundary condition that is applied,
- (5) if at the onset of failure  $\sigma \geq \sigma_f$ , then the failure wave follows the physical boundary and  $\sigma$  is not constrained, and
- (6) when an internal failure-wave boundary crosses the physical boundary, the failure calculation is ended after  $\kappa < \kappa_f$ .

The default value of  $\sigma_f$  is  $\sigma_c$  (i.e., the sonic angle).  $\kappa_f$  has no default value and always needs to be entered. We will demonstrate the properties of this model by considering some examples.

## (2) Examples

All the calculations that we describe use  $D = 0.8 + 0.2(1 - \kappa/\kappa_f)$ . We give the input file for the first example only (Table B.1).

---



---

**TABLE B.1. INPUT FILE di4a2fl**

---



---

```

'run'  'Corner Turning(plane sym)'
!      Plane initial, hard right, two-side
'fluid' 3.0, 0.0
'Dkap'  3  1.00  0.80  0.50      !failure
'edgel'  3  0.0  0.0  0.0  7.00    !file dp8crn
'edger'  3  2.0  0.0  0.0  7.00    !file dp9crn
'xnet'   0.0 64  2.0
'tnet'   0.0 4  2.00
'tnet'   0.0 8 16.0
'ic'     1  0.0      !line
'bcl'    3  0.50      !sonic
'bcr'    3  0.50      !sonic
'bcr't'  1              !hard
'twav'   1  0.0625     !twave(left bndry)
'dials'  0.25 0.001 0.000001

```

---



---

Example 1 (data file di4a2f1 and Fig. B.1) shows detonation extinction in slab geometry. The detonated explosive occupies the roughly "triangular" region whose corners are at:  $(x = 0, y = 0)$ ,  $(x = 2, y = 0)$ , and  $(x = 1, y = 6)$ . Initially the shock is flat ( $0 \leq x \leq 2, y = 0$ ) and running at  $D = 1$ . The failure waves that enter the system at  $(x = 0, y = 0)$  and  $(x = 2, y = 0)$ , continually erode the detonation until at  $t = 6.7$  the detonation is totally quenched. The chain-dot lines are the failure-wave loci. The shock loci are shown at  $t = 0, 2, 4, 6$ . The dashed line is the track of a right-facing acoustic wave coming from the corner at  $(x = 0, y = 0)$ . This problem used the parameter values  $\kappa_f = 1.0$ ,  $\sigma_f = 0.5$ , and  $\sigma_c = 0.5$ .

Example 2 (Fig. B.2) retains the parameters of Example 1 with the exception that  $\kappa_f$  is increased to  $\kappa_f = 2.0$ . Now the failure waves can propagate into the explosive only a limited distance. They are turned out at  $t = 1.14$  and are flushed from the system at  $t = 3.0$ . Two small "dead" regions remain as the detonation proceeds up the slab. This calculation ends at  $t = 7.0$ , at which time the detonation is about to enter the large piece of explosive occupying the region above  $y = 6.66$ . The shock loci are shown at  $t = 0, 1, 2, 3, 4, 5, 6, 7$ .

Example 3 (Fig. B.3) uses the same parameters as Example 2. The plotting scale is compressed. As the detonation emerges from the thin slab (see Fig. B.2 for a detailed picture of the slab) into the large piece of explosive, it has great difficulty turning the  $90^\circ$  corner. The detonation drives forward, spreading sideways only slowly. Most of the explosive remains undetonated. This contrasts sharply with the perfect corner turning of a Huygens wave. The shock loci are shown at  $t = 0, 2, 4, 6, 8, 10, 12, 14, 16$ .

Example 4 (Fig. B.4) uses the parameter values  $\kappa_f = 2.0$ ,  $\sigma_f = 0.2$ , and  $\sigma_c = 0.2$ . These differ from the parameters in Example 2 in that both  $\sigma_f$  and  $\sigma_c$  are reduced. The principal effect of this change is to decrease the speed of the failure waves along the shock. Now as the detonation enters the large piece of explosive occupying  $y \geq 6.66$ , the detonation spreads reasonably well. Two "dead" semi-elliptical zones remain at the corners. As observed experimentally, the first arrival of the detonation along lines of constant  $x$  occurs for  $y > 6.66$ , where the horizontal boundary is at  $y = 6.66$ . The shock loci are shown at  $t = 0, 2, 4, 6, 8, 10, 12, 14, 16, 18$ .

Example 5 (Fig. B.5) uses the same parameters as does Example 2, except that the geometry is axisymmetric. The most notable difference is the size of the "dead" zone: a cylindrical shell of explosive remains undetonated.

### (3) Parameter Calibration

Our detonation-failure model qualitatively reproduces some of the well known features of extinction. Since no theoretical support exists for its use, it should be viewed as a phenomenological model. Nonetheless, when properly calibrated it can be a useful tool to help us predict when undesirable features such as "dead" zones will appear. We now consider a possible calibration strategy.

Of the two new parameters ( $\kappa_f$  and  $\sigma_f$ ) that we require,  $\kappa_f$  can be obtained from “rate stick” data taken near the “failure diameter.” This is obtained as part of the  $D(\kappa)$  calibration to steady-state data. The failure-wave spreading parameter,  $\sigma_f$  can only be inferred from a time-dependent experiment. The corner-turning experiment shown in Fig. B.4 can be used to estimate  $\sigma_f$ . A highly-resolved numerical simulation of failing detonation would also yield some insights. Clearly we expect that  $\sigma_f \leq \sigma_c$ , because the speed of the failure wave should not exceed the acoustic speed.

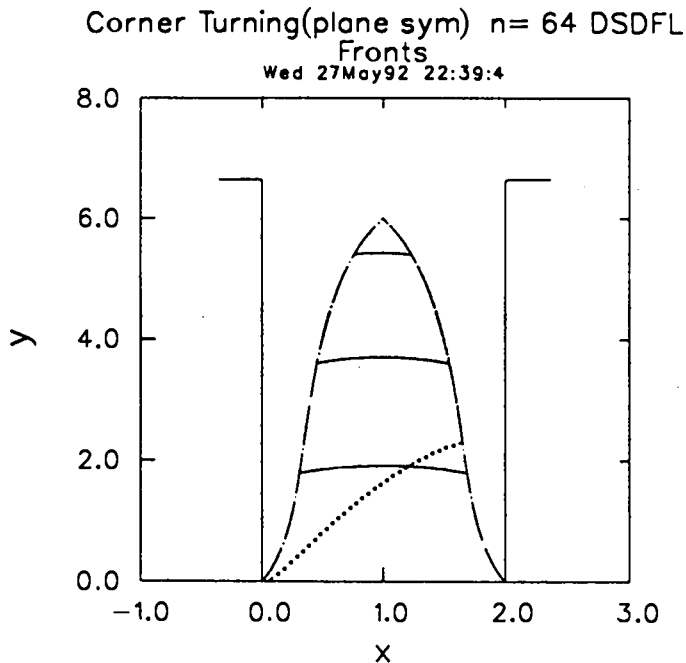


Fig. B.1 The shock fronts for Example 1, showing detonation extinction in an explosive slab. Only the central “triangular” region detonates.

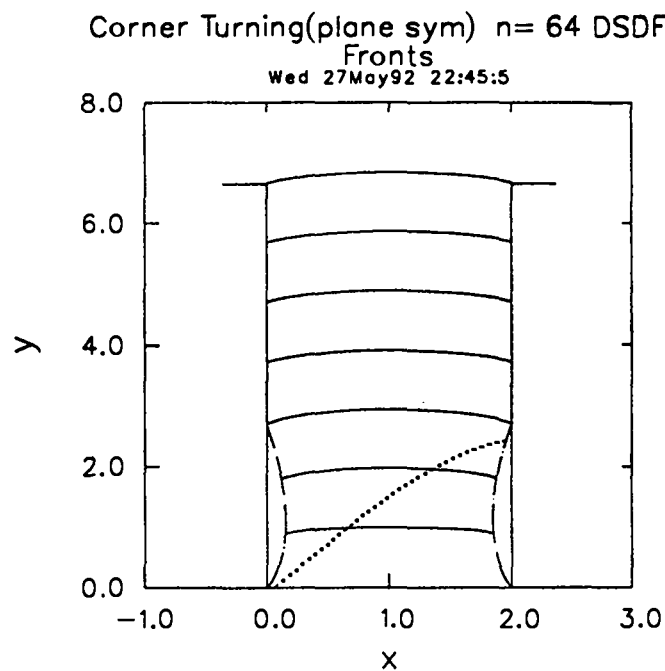


Fig. B.2 The shock fronts for Example 2. Small "dead" zones are found near the input face  $y = 0$ . Most of the explosive slab detonates.

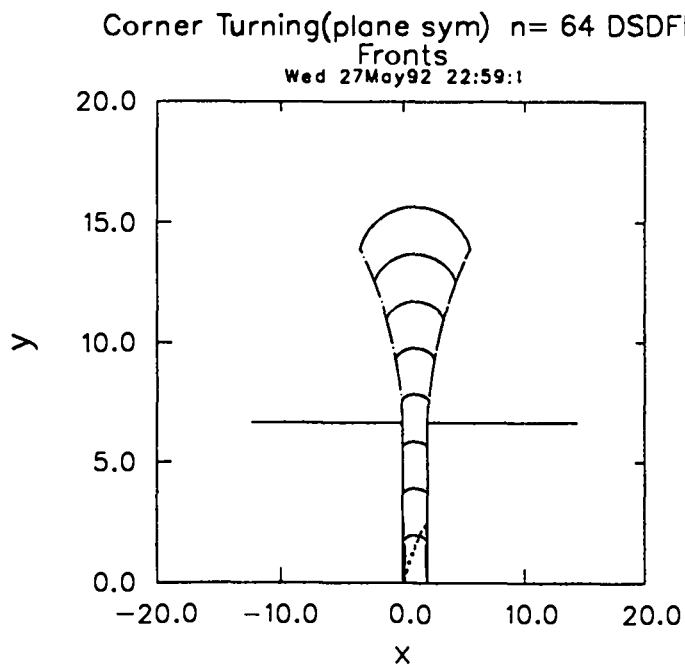


Fig. B.3 The shock fronts for Example 3. As the detonation emerges into large piece of explosive above  $y = 6.66$ , it is unable to turn the corner. Much of the material remains undetonated. The parameters are those of Example 2.

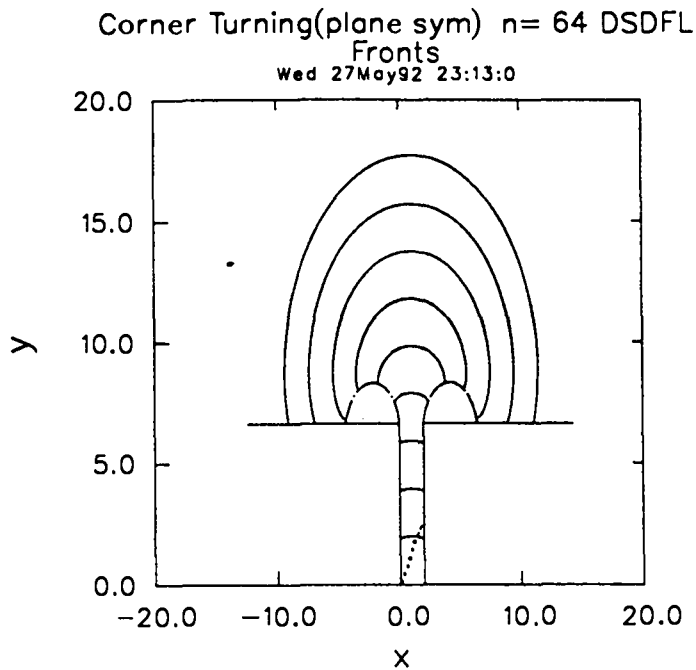


Fig. B.4 The shock fronts for Example 4. When  $\sigma_f$  and  $\sigma_c$  are decreased from the values used in Example 2 (i.e., setting  $\sigma_f = \sigma_c = 0.2$ ), the detonation turns the corner. Only small regions of "dead" explosive are left behind.

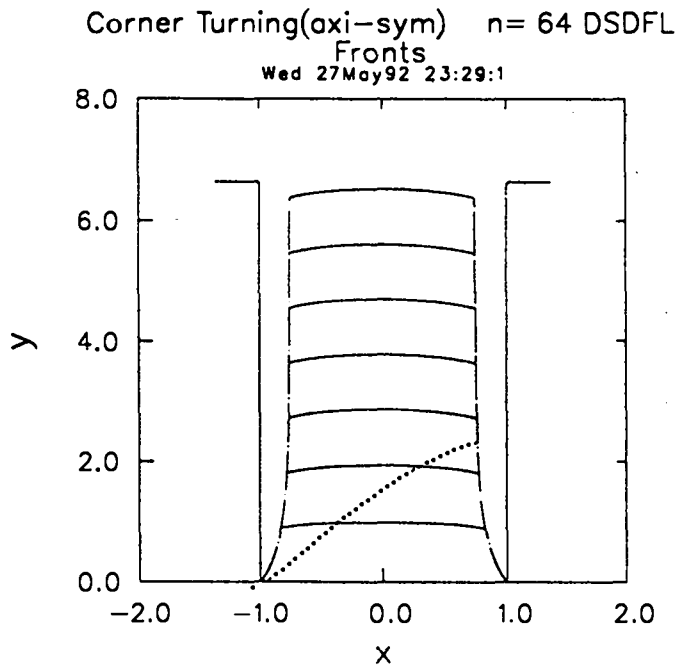


Fig. B.5 The shock fronts for Example 5. This is an axisymmetric problem that uses the parameters of Example 2. A cylindrical shell of explosive remains undetonated.

**This report has been reproduced directly from the best available copy.**

**It is available to DOE and DOE contractors from the Office of Scientific and Technical Information, P.O. Box 62, Oak Ridge, TN 37831. Prices are available from (615) 576-8401, FTS 626-8401.**

**It is available to the public from the National Technical Information Service, U.S. Department of Commerce, 5285 Port Royal Rd., Springfield, VA 22161.**

